MASTER DEGREE THESIS

Department of Control and Computer Engineering

Mechatronic Engineering

a.y. 2023/2024

Study and development of an ergonomic haptic interface using flexible coils

Supervisors:
Alessandro RIZZO
(*PoliTO - DET*)
Domenico PRATTICHIZZO
(*UniSi - DIISM - SIRSLab*)

Co-supervisors:
Tommaso LISINI BALDI
(*UniSi - DIISM - SIRSLab*)
Leonardo FRANCO
(*UniSi - DIISM - SIRSLab*)

Candidate:
Morgan CASALE

July 2024

POLITO

Abstract

Department of Control and Computer Engineering

Mechatronic Engineering

Study and development of an ergonomic haptic interface using flexible coils

The world of haptic is an emerging field of research with rapidly evolving technologies. Researchers are still looking for the optimal solution to create a haptic device that can provide a realistic touch sensation. Vibrations, forces, and temperatures are the stimuli involved in the majority of the touch experience. For what concerns the rendering of texture, i.e., generating vibratory cues, the most widespread technology is high-performance piezo actuators, but even this technology has multiple limitations. The most critical ones are their limited capability of generating low-frequency responses and their lack of flexible models. These characteristics are crucial for the creation of a realistic haptic interface that could also be easily integrated into wearable devices.

This thesis aims at investigating the use of flexible PCB coils in haptic applications. Flexible PCB coils are a new technology which can be used to create voice actuator-style haptic interfaces that can withstand bending stresses and produce low-frequency vibrations. Voice-coil actuators are systems based on the electromagnetic force interaction between a coil and a magnet. This force can be harnessed with the use of a membrane to transfer vibrations to human skin.

The first part of the thesis focuses on the physics of such a device with the creation of a mathematical model of the entire force transmission chain, considering also how finger-pulp skin reacts to the device stimuli at different frequencies and amplitudes.

Next, the electronics required to drive the proposed device is presented.

Finally, the last part reports the design and testing of a series of prototypes that will help us understand the limitations and potential of this technology.

Contents

List of Figures

List of Tables

List of Abbreviations

RMS	**R**oot **M**ean **S**quare
PCB	**P**rinted **C**ircuit **B**oard
AC	**A**lternated **C**urrent
DC	**D**irect **C**urrent
re	**re**ferring to
PLA	**P**oly**L**actic **A**cid
ABS	**A**crylonitrile **B**utadiene **S**tyrene
TPU	**T**hermo**P**lastic **U**rethane
BVOH	**B**utylene **V**inyl **O**l**H**exanoate
FEM	**F**inite **E**lement **M**ethod

List of Symbols

m	**m**eter	Distance
s	**s**econd	Time
Hz	**H**ertz	Frequency
dB	**D**ecibel	Intensity
g	**g**ram	Mass
N	**N**ewton	Force
Pa	**Pa**scal	Pressure
V	**V**olt	Electrical Voltage
A	**A**mpere	Electrical Current
W	**W**att	Electrical Power
Ω	Ohm	Electrical Resistance
F	**F**arad	Electrical Capacitance
H	**H**enry	Electrical Inductance
T	**T**esla	Magnetic Flux Density
Wb	**W**e**b**er	Magnetic Flux

Chapter 1

Introduction

1.1 Thesis objective

The world of haptics is an exciting field in the world of robotics, it was born from the will to bridge even further the digital world with the real one. After digitalizing the sense of sight and hearing, the sense of touch is the next logical frontier to conquer. The sense of touch is a very important sense for humans, it is the first sense that develops in the womb and it is the first sense that is used by a newborn to explore the world. It is also the sense that is the most difficult to replicate in a virtual environment.

In past years there has been a lot of research in the field of haptics, but the field is still in its infancy. Even if the current best haptic devices are able to provide vibration, force and temperature cues to the user, they are still far from being able to replicate the sense of touch realistically.

The most important components of haptics are vibrations and forces, they are the most common cues that are used to convey information to the user. The generation of these types of cues is usually handled by piezoelectric actuators as they can generate vibrations with a high bandwidth (especially in the high range) and precision exerting notable force.

The only drawbacks of piezoelectric actuators are that they are rigid components, they cannot be bent or stretched, and they are not able to generate forces in the low range.

The objective of this thesis is to study a different type of actuator, voice coils based on flexible coils, and to compare them with piezoelectric actuators. The main advantage of voice coils is that they can generate vibration with enough force also at low frequencies. In this research, we want to understand if we can create a haptic device that can be stretchable and possibly wearable by using flexible coils.

We will study the strengths and weaknesses of such type of actuator and propose multiple designs for a haptic device created with this technology.

1.2 Thesis structure

The thesis is structured in further five chapters:

Chapter 2 - *Background*:
    This chapter provides a comprehensive overview of all physical laws and phenomena that need to be known to describe the working principle of a voice

actuator style haptic actuator based on flexible PCB technology. The chapter covers the basics of the electromagnetism laws that will be used to describe the magnetic field generation of the coil and its interaction with a magnet to produce mechanical force. We will then talk about Flexible PBC coils physical characteristics, strengths and flaws.

Chapter 3 *- Overview of Haptic Feedback*:
This chapter provides an overview of haptic feedback talking about how the haptic human perception works and its limits. We will then talk about the leading technology used in haptic feedback devices and its strengths and weaknesses.

Chapter 4 *- Powering circuit design*:
This chapter explains the design procedure for the entire control system for the haptic actuator. We will start by describing the controller characteristics and used hardware, then we will talk about a possible design for the power amplifying circuit.

Chapter 5 *- Implementation and Prototypes*:
This chapter presents all the prototypes we have built and tested during the development of the haptic actuator. Starting from a simple testbed for planar coils, we will then talk about a more advanced wearable prototype to finally pass to a flexible prototype. For each prototype, we will describe the design choices, the building process, their strengths and issues.

Chapter 6 *- Discussions and Conclusions*:
In this last chapter, we will discuss the results obtained from the prototypes and the possible future developments of the technology. We will also talk about the other applications of PCB coils.

Chapter 2

Background

2.1 Magnetic Coils

2.1.1 Brief History

The **connection between electricity and magnetism** was first demonstrated by Hans Christian Oersted in 1820 when he observed that an electric current flowing through a wire could deflect a nearby magnetic needle.

Meanwhile, the creation of the **first practical electromagnet** is credited to William Sturgeon and André-Marie Ampère who, after Oersted's discovery, experimented with creating coil windings wrapped around an iron core which allowed them to achieve much stronger magnetic fields.

During the 1830's Michael Faraday's discovery of electromagnetic induction further advanced the understanding of magnetic fields and coils. Faraday demonstrated that a **changing magnetic field could induce an electric current in a nearby conductor**, laying the groundwork for transformers and modern electrical generators.

The latter half of the 19th century saw rapid advancements in electrical engineering. Innovations like early **electric generators** (dynamos), **transformers**, and **electric motors** heavily **relied on magnetic coils** for their operation. Researchers such as Nikola Tesla and Thomas Edison further developed these technologies.

Magnetic coils continue to play a vital role in various fields, including **power generation**, **telecommunications**, **electronics**, and **medical imaging** (such as MRI machines). With advancements in materials science and manufacturing techniques, magnetic coils have become more efficient, compact, and versatile.

In recent years, as the use of **PCBs** has become widespread, researchers started experimenting with **creating coil windings utilizing this technology**.

2.1.2 Physics of inductors

We will start this thesis by analyzing all the physics laws that govern the behavior of induction coils. This will allow us to understand their behavior with magnetic field generation and the power cost for their operation.

Inductance

All **conductors have some inductance**, which may have either desirable or detrimental effects in practical electrical devices. The inductance of a circuit depends on

the **geometry of the current path** and the **magnetic permeability** of **nearby materials**.

The **inductance** of a circuit depends on the **magnetic flux** and **current** flowing through it:

$$L = \frac{\Phi(i)}{i}$$

Where:

- L is the inductance [H].

- i is the current [A].

- $\Phi(i)$ is the magnetic flux through the circuit [Wb].

Reactance

When a current signal is applied to an inductor, a flux is generated. Then, considering Faraday's law of induction, any **change in flux** through a circuit induces an **electromotive force** $\mathcal{E}$, proportional to the rate of change of flux:

$$\mathcal{E} = -L\frac{d\Phi(t)}{dt}$$

We also know that by Lenz's law, the voltage across the inductor can be calculated as:

$$V = -L\frac{di}{dt}$$

Inductors resist changes in current due to the magnetic field they generate when current passes through them. When we apply a **sinusoidal signal** to our inductor, the current will be continuously **changing direction**. The **inductor's opposition** to these changes is represented as **reactance**.

Inductive reactance (X_L) is measured in ohms and is calculated using the formula:

$$X_L = 2\pi f L$$

Where:

- X_L is the inductive reactance [Ω]

- f is the frequency of the AC current [Hz]

- L is the inductance of the inductor [H]

We can then calculate the total impedance of the inductor as

$$Z = \sqrt{R^2 + X_L^2}$$

Where:

- Z is the total impedance [Ω]

- R is the resistance of the inductor [Ω]

- X_L is the inductive reactance [Ω]

Joule heating

Any passive component in an electrical circuit will dissipate power in the form of heat. This is known as **Joule heating** and is caused by the resistance of the component.

The power dissipated in an inductor is given by the relation

$$P = |I_{RMS}|^2 R = \frac{|V_{RMS}|^2}{|Z|^2} R \tag{2.1}$$

Where:

- P is the power dissipated in the inductor [W]

- I is the current flowing through the inductor [A]

- R is the resistance of the inductor [Ω]

- V is the voltage across the inductor [V]

- Z is the total impedance of the inductor [Ω]

Definition of Root Mean Square (RMS) values

As we have seen in the previous paragraphs, the **power dissipated** by the coil depends on the **root mean square values** of the **current** and **voltage**. We use the **RMS values** because they **allow us to compare** the power dissipated by the coil when powered in **AC** and **DC** conditions.

For DC signals these values are equal to the DC one, while for sinusoidal signals V_{RMS} can be calculated as:

$$V_{RMS} = \sqrt{\frac{1}{T} \int_{T}^{0} [f(t)]^2 \, dt}$$

Where:

- T is the period of the input signal

- $f(t)$ is the function of the signal

Then in case we're dealing with AC signals having a DC offset we can use the formula

$$V_{RMS_{AC+DC}} = \sqrt{V_{DC}^2 + V_{RMS_{AC}}^2}$$

Some formulas for important waveforms:

Name	Waveform	V_{RMS}
DC	V_P	V_P
Sine Wave $[-V_P, V_P]$	$V_P \sin(2\pi f t)$	$\frac{V_P}{\sqrt{2}}$
Polarized Sine Wave $[0, V_P]$	$\frac{V_P}{2}(\sin(2\pi f t) + 1)$	$\frac{V_P}{2}\sqrt{\frac{3}{2}}$
Square Wave $[-V_P, V_P]$	$V_P \text{sgn}(\sin(2\pi f t))$	V_P
DC-shifted Square Wave $V_{DC} + [-V_P, V_P]$	$V_{DC} + V_P \text{sgn}(\sin(2\pi f t))$	$\sqrt{V_{DC}^2 + V_P^2}$

FIGURE 2.1: RMS values for different waveforms.

2.1.3 Magnetic field generation
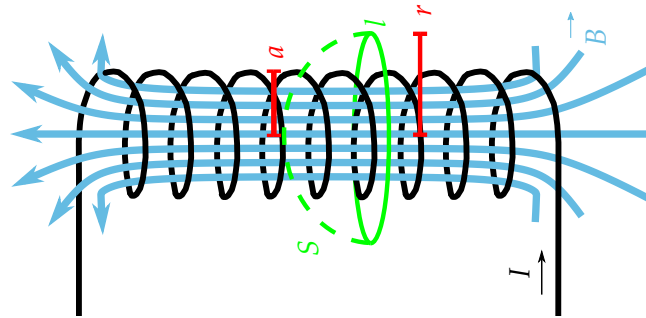
FIGURE 2.2: Magnetic field generated by a solenoid.

The strength of the magnetic field on the z-axis of the coil is derived from the Biot-Savart Law and is given by the formula

$$B_z = \frac{N\mu I r^2}{2(r^2 + z^2)^{\frac{3}{2}}} \tag{2.2}$$

Where:

- B_z is the magnetic field on the z-axis [T].

- μ is the magnetic permeability of the medium [H/m].

- I is the current flowing through the wire [A].

- r is the radius of the coil [m].

- N is the number of turns of wire in the coil.

- z is the z-distance from the center of the coil [m].

Usually, coils are paired with a core material to increase the magnetic field intensity; in that case, instead of the permeability of air, the permeability of the core is calculated as

$$\mu = \mu_0 \cdot \mu_r$$

where μ_r is the relative permeability of the core material.

With the right material for the core, the magnetic field intensity can be highly increased compared to the field generated by the coil alone.

Magnetic Flux and Field relation

We can also relate the magnetic field to the magnetic flux generated by the coil. The magnetic flux is given by the formula

$$\Phi_B = B \cdot A$$

Where:

- Φ_B is the magnetic flux [Wb].

- B is the magnetic field [T].

- A is the area of the coil [m^2].

2.2 PCB Coils

The **biggest problem with standard coils is their size**, especially in the z-direction as the more windings are used the thicker they will become. This is a problem for applications where space is limited, such as in the case of implantable devices. To address this issue, researchers have started to experiment with **creating coil windings using PCB technology**. This allows for the creation of **coils** that are **thinner** and **more compact** than traditional coils. In this section, we will discuss the different types of PCB coils and the challenges associated with their miniaturization.

2.2.1 Planar coils

As PCBs are 2D objects we can't work on the z-axis to create the coil's windings. This means that the **windings** have to be created **on the same plane**. In 1984 researchers from Osaka University proposed the first implementation of a possible solution in the form of planar coils.

They proposed and tested a **structure comprised of concentric spirals**, with different shapes, made of a **conductive material** (mostly copper) **suspended in an insulation material** and then covered by two high magnetic permeability material layers[1].
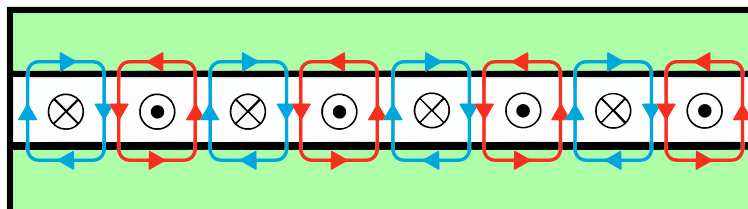
FIGURE 2.3: Internal structure of a planar coil.

With the mainstream adoption of PCBs in the electronics industry, researchers have created planar coils using PCBs by etching **spiral patterns** on the **copper layer**. This allowed for the **production** of planar coils **easily** and **cheaply**.

The main advantage of planar coils is that they can be **easily integrated into the PCB design**, reducing the overall size of the device. This is particularly useful in the case of wireless power transfer systems, where the coils are used to transfer power between devices. The **smaller size** of the coils allows for more **compact** and **portable devices**.

Another advantage is the ability to design coils of **arbitrary shapes and sizes**, depending on the requirements of the application. This flexibility allows for the creation of coils that are optimized for specific applications and PCB shapes, resulting in improved performance.
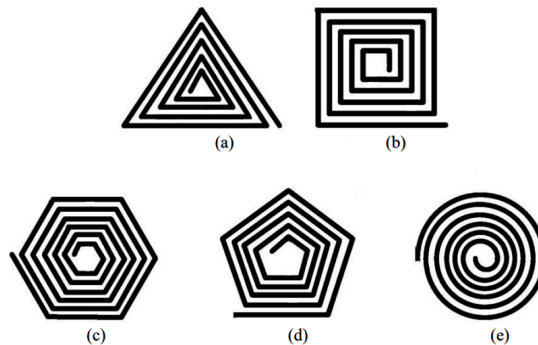
FIGURE 2.4: Some possible planar coil architectures. (a) Triangle, (b) Square, (c) Pentagon, (d) Hexagon, (e) Circle.

2.2.2 Planar coil magnetic field

The structure of a planar coil is very different from a standard one, as it is a flat structure with a spiral winding. The magnetic field generated by a planar coil is more complex than that of a standard coil, as the **magnetic field is not concentrated in the center** of the coil but is distributed over the entire surface of the coil. This makes the magnetic field generated by a planar coil more difficult to calculate than that of a standard coil.
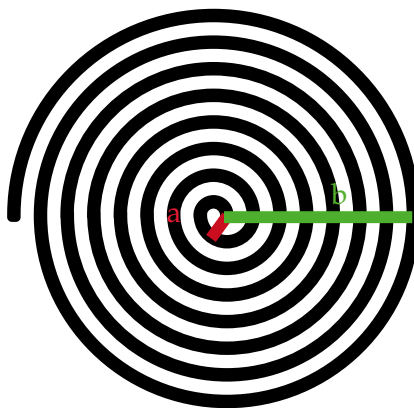
FIGURE 2.5: Circular spiral coil.

An open-closed equation is difficult to derive so, usually, the equation for the magnetic field generated by a coil on its surface is simplified as:

$$Bz = \frac{\mu NI}{2} \cdot \frac{\ln(\frac{b}{a})}{b-a} \tag{2.3}$$

Where:

- Bz is the magnetic field on the z-axis [T]
- μ is the magnetic permeability of the medium [H/m]
- N is the number of turns of the spiral
- I is the current flowing through the wire [A]
- b is the external radius of the spiral [m]
- a is the internal radius of the spiral [m]

To then find the magnetic field at a distance z from the center of the coil, we can use the equation 2.2 from the previous subsection and substitute the radius r of the coil with

$$r' = \frac{b-a}{\ln \frac{b}{a}} \rightarrow B_z = \frac{\mu NIr'^2}{2(r'^2 + z^2)^{\frac{3}{2}}} \tag{2.4}$$

Where:

- r' is the average radius of the spiral [m]
- z is the distance on the z-axis from the center of the coil [m]

2.2.3   Multi-layer PCB coils

Another approach to miniaturizing PCB coils is to create **multi-layer coils**. This is done by stacking **multiple layers** of **PCBs** on top of each other, with each layer containing a different part of the coil. This allows for the creation of coils with a **higher number of windings** in a **same space**. The **main challenge** with multi-layer PCB coils is the **alignment of the different layers**. If the layers are not aligned properly, the coil will not function correctly.

Current manufacturing allows for up to 10 layers of PCBs to be stacked on top of each other. However, the more layers that are added, the more difficult it becomes to align the layers correctly. If the layers are not aligned properly, the **magnetic field** generated by each layer will also **not be aligned**, which can lead to a **decrease in the efficiency** of the coil due to **interferences**.

Total inductance

Considering a two layers coil the total inductance can be calculated as:

$$L_s = 2L_0 + 2M, M = K_c \cdot L_0$$

Where:

- L_s is the total inductance of the coil [H].

- L_0 is the inductance of a single layer [H].

- M is the mutual inductance between the two layers [H].

- K_c is the coupling coefficient between the two layers.

Then K_c can be calculated with an empirical formula derived from multiple measurements by *Jonsenser Zhao* [2] as

$$K_c = \frac{N^2}{0.64[(0.184d^3 - 0.525d^2 + 1.038d + 1.001)(1.67N^2 - 5.84N + 65)]}$$

Where:

- N is the number of turns of the coil.

- d is the distance between the two layers [m].

Magnetic field generated by a Multilayer coil

We can use equation 2.1.2 and L_s, calculated in the previous point, to find the magnetic flux through the coils

$$\Phi(I) = L_s \cdot I$$

Then with equation 2.1.3 we can derive the total magnetic field as

$$B_t = \frac{L_s \cdot I}{\pi r^2}$$

Where:

- B_t is the total magnetic field [T].

- r is the radius of the coil [m].

2.3 Flexible PCB coils

Flexible PCB coils are a type of PCB coil that is made using a **flexible substrate**. This allows for the creation of coils that **can be bent** and **twisted without breaking**.

2.3.1 Pros of flexible coils

Flexible PCBs offer several advantages over traditional rigid PCBs, we can list some of the key pros of flexible PCBs:

1. **Flexibility and Space Savings**: Flexible PCBs can bend and twist, allowing for **compact** and **efficient use of space** in electronic devices.

2. **Lightweight**: The materials used in flexible PCBs are **lightweight**, making them ideal for applications where weight is a concern, such as in aerospace or portable electronics.

3. **Improved Design Freedom**: Flex PCBs allow for more creative and versatile designs because they can be **formed into complex shapes** and **fit** into **tight** or **irregular spaces**.

4. **Reduced Connectors and Interconnects**: Because flexible PCBs can bend, they can often **eliminate** the **need** for **additional connectors and interconnects**, reducing overall system complexity.

5. **Vibration and Shock Resistance**: Flexible PCBs can **absorb shock** and **vibrations better than rigid PCBs**, making them suitable for use in environments where these are concerns.

6. **Simplified Assembly**: With fewer connectors and interconnects, assembly becomes easier and faster, reducing labor and potential points of failure.

2.3.2 Application challenges

As said before flexible PCBs offer great design flexibility and the possibility of implementing innovative designs and devices but they also come with their own set of **challenges**; especially in the case of flexible coils.

Rise of high resistance

Taking as an example the flexible coil we'll be using in our project, the resistance of the coil is about 30Ω. This is a relatively **high resistance** for such a small coil, especially when compared to traditional copper wire ones. This is due to the intrinsic structure of PCBs, especially flexible ones. PCBs are created by etching very **thin copper traces** on a substrate, in the case of flexible PCBs, as the substrate must be flexible, their **thickness is even lower** and consequently also the traces are.

The coil can be considered as a very long strand of a very thin copper so its resistance can be calculated using the Ohm Law

$$R = \rho \cdot \frac{L}{A}$$

Where:

- R is the resistance [Ω].

- ρ is the resistivity of the material [$\Omega \cdot m$].

- L is the length of the conductor [m].

- A is the cross-sectional area of the conductor [m^2].

Then to find the length of the copper traces we can use the approximated formula [3]

$$L = N\pi\frac{D + d}{2}$$

Where:

- N is the number of turns.

- D is the outer diameter of the coil [m].

- d is the inner diameter of the coil [m].

The tracks' cross-section is a **rectangle** so the area can be calculated as

$$A = w \cdot t$$

Where:

- w is the width of the track [m].

- t is the thickness of the copper [m].

Finally considering the physical characteristics of our coil

Coil Specifications	
Track (width/spacing)	$4/4mil = 1.016 \cdot 10^{-4}/1.016 \cdot 10^{-4}m$
Turns	2*35 (two coils in series)
External radius	$6.86 \cdot 10^{-3}m$
Copper thickness	$0.5oz = 1.74 \cdot 10^{-5}m$
Resistivity	$1.72 \cdot 10^{-8}\Omega m$
Maximum Constant Power	$0.8W$

TABLE 2.1: Physical characteristics of a Flexar coil

The Length of the tracks (considering both spires) will be $L = 3.4548m$ and the cross-section area will be $A = 1.7678 \cdot 10^9 m^2$. As we can observe we have a wire that is both very long and very thin so a high resistance is expected (from the calculation $R = 33.61\Omega$).

Also, the resistance of the coil is **dependent on the Temperature** of the coil, as the **temperature increases** the **resistance** of the copper **increases** as well. This is because the resistivity of copper increases with temperature. This is a problem as the coil releases a **lot of heat** when powered with **high currents**.

The temperature coefficient of resistivity of copper is $\alpha = 0.003862 \frac{1}{°C}$ so the resistivity of copper at a certain temperature can be calculated as

$$\rho(T) = \rho_{T_{ref}} \cdot (1 + \alpha \cdot (T - T_{ref}))$$

Where:

- $\rho_{T_{ref}}$ is the resistivity at the reference temperature $[\Omega \cdot m]$.

- α is the temperature coefficient of resistivity $[\frac{1}{°C}]$.

- T is the temperature $[°C]$.

- T_{ref} is the reference temperature $[20\ °C]$.

Joule effect

As said before, a coil of this type releases a lot of heat when powered with high currents. This is also due to its high resistance.

The heat dissipated by a coil can be calculated using the formula

$$P = I_{RMS}^2 R = \frac{V_{RMS}^2}{R}$$

Where:

- P is the power dissipated by the coil [W].

- I_{RMS} is the root mean square current [A].

- V_{RMS} is the root mean square voltage [V].

- R is the resistance of the coil $[\Omega]$.

The coil can dissipate a maximum of 0.8W of power, this is a very low value and it is very easy to surpass it. This is a problem as the coil can be **damaged** if it dissipates more power than it can handle.
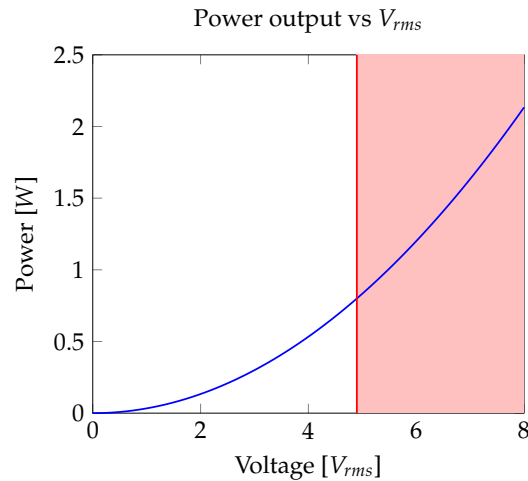
FIGURE 2.6: Power profile of a Flexar coil

When exceeding the limit, even if the coil doesn't get damaged, the heat it releases can affect the **performance** of the coil. As the coil's resistance increases with temperature, the coil will dissipate even more power, this can lead to a **thermal runaway** situation where the coil will keep increasing its temperature until it gets damaged.

The only solution could be to introduce a **heat sink** to dissipate the heat but for the amount needed to be managed, heat sinks must be quite **bulky** and flexible solutions are not up to the task.

Magnetic field strength

As the coil can't be run at high currents, the **magnetic field** it generates will be **very weak**.

Considering the Flexar coil as an example we can plot the magnetic field strength, at the surface, as a function of the voltage applied to the coil using equation 2.3 (considering the coil as a series of two spirals)

FIGURE 2.7: Flexar magnetic field profile

As we can observe even at the power limit of 0.8W ($\simeq 5V$) the magnetic field generated by the coil is **very low** ($\simeq 4mT$).

Resistance parasitic effects due to AC current

This paragraph will be a brief introduction to the **parasitic effects** that can occur in a coil due to the **AC current** that flows through it. All these effects are **negligible at low frequencies** (up to about 1kHz) which is the range we are aiming for in this project, but we will explore them for the sake of future research.
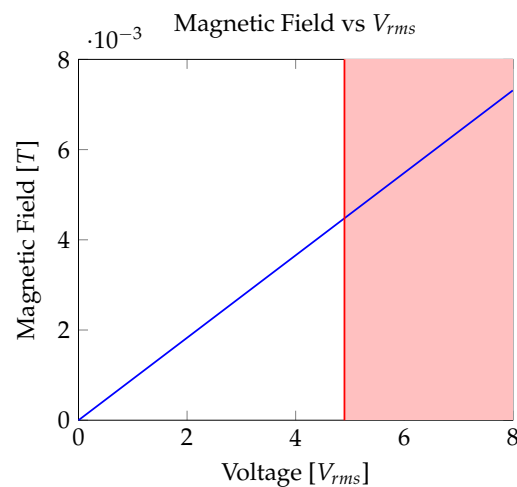
The main parasitic effects that can occur in a coil are:

- **Reactance:** This is the opposition that a coil offers to the flow of AC current. This is due to the self-inductance of the coil which opposes the change in current flowing through it. This effect can lead to a change in the effective resistance of the coil.

  The reactance of a coil can be calculated using the formula

  $$X_L = 2\pi f L$$

  Where:

  - X_L is the reactance of the coil [Ω].
  - f is the frequency of the AC current [Hz].
  - L is the inductance of the coil [H].

  Then the impedance of the coil can be calculated as

  $$Z = \sqrt{R_{DC}^2 + X_L^2}$$

- **Skin effect:** This effect is due to the current flowing through a conductor tending to flow on the **surface** of the conductor. This gives rise to a **thin layer inside the conductor where all the current flows**. As a result, the effective resistance of the conductor **increases**. This effect is more pronounced at **higher frequencies**.
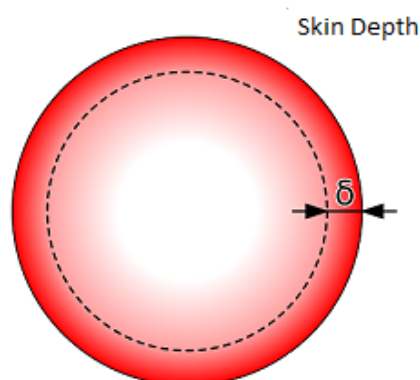
FIGURE 2.8: Representation of the thin surface generated by the skin effect

The thickness of this area is called the **skin depth** and can be calculated using the formula

$$\delta = \sqrt{\frac{\rho}{\mu \pi f}}$$

Where:

- δ is the skin depth [m].

- ρ is the resistivity of the conductor [$\Omega \cdot m$].

- μ is the magnetic permeability of the medium [H/m].

The effective resistance of the conductor can be derived from the skin depth using Dowell's equation [4]

$$R_{skin} = F_{skin} \cdot R_{DC}$$

and

$$F_{skin} = \frac{1}{2}\left(\frac{h}{\delta}\right) \frac{\sinh(\frac{h}{\delta}) + \sin(\frac{h}{\delta})}{\cosh(\frac{h}{\delta}) - \cos(\frac{h}{\delta})}$$

Where:

- R_{skin} is the effective resistance of the conductor due to the skin effect [Ω].

- F_{skin} is the skin effect factor.

- h is the thickness of the conductor [m].

Simulating the skin effect function in the case of Flexar's coils (using the values specified in table 2.1), we can observe in graph 2.9, that the skin effect is **negligible** up to $10^8 Hz$ as the **thickness** of the flexible PCB's **traces** is **very low**.
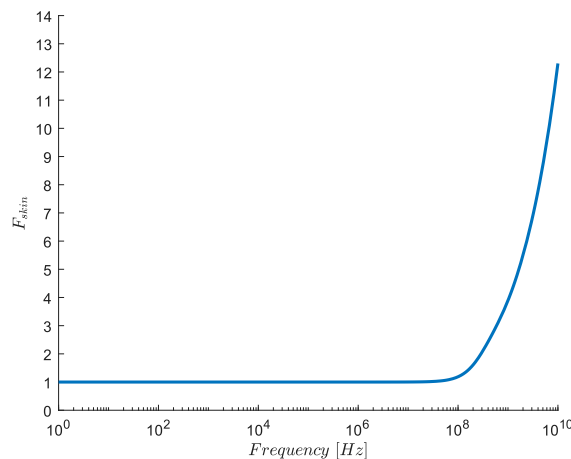
FIGURE 2.9: Logarithmic plot of the skin effect factor for a flexible PCB coil

But we can observe from graph 2.10 that the study done on thicker traces'
(0.5mm) coils resulted in the skin effect starting to curve upwards already at
$10^5 Hz$.
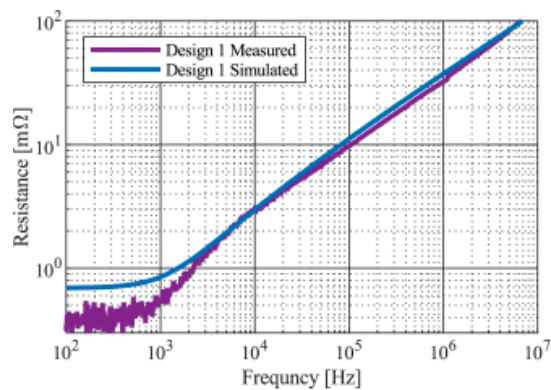
FIGURE 2.10: Skin effect on thicker traces [5]

- **Proximity effect:** This effect is similar to the skin effect but it occurs when two
  conductors are close to each other. The current flowing through one conductor
  induces an **eddy current** in the other conductor which can lead to a change in
  the effective resistance of the conductors.
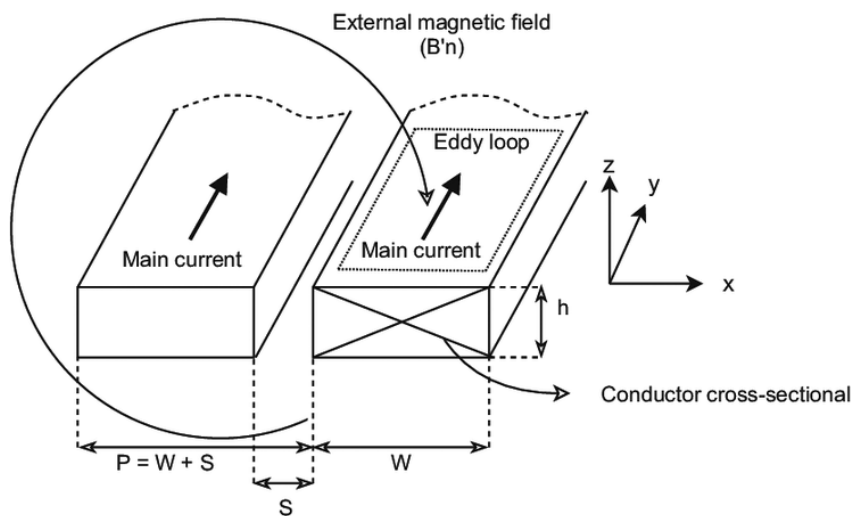
FIGURE 2.11: Representation of the proximity effect

The contribution of the proximity effect to the effective resistance of the coil can be calculated using the formula (considering current flowing in the coil $I_{ex} = 1A$) [6]

$$R_{proximity} = \frac{1}{12}h\sigma\pi^2 f^2 B_n^2 w^3$$

Where:

- σ is the conductivity of the conductor $[\Omega^{-1} \cdot m^{-1}]$.
- h is the thickness of the conductor [m].
- f is the frequency of the AC current [Hz].
- B_n is the average external magnetic field [T].
- w is the width of the conductor [m].

We can also approximate $F_{proximity}$ ($F_{proximity} = R_{proximity}/R_{DC}$) as

$$F_{proximity} = \frac{F_{skin}}{3}$$

So when the contribution of the skin effect is negligible, the proximity effect will be **negligible** as well.

2.3.3 Running flexible PCB coils

High current needs

As discussed in the previous paragraph flexible coils have very high resistance so to produce even low magnetic fields **high current** must be provided. Considering the power limit of the Flexar coil $P_{max} = 0.8W$ we can calculate the maximum current that can be provided to the coil with 2.1 as

$$I = \sqrt{\frac{P_{max}}{R}} = \sqrt{\frac{0.8}{30}} = 0.1633A$$

Constant Voltage vs Constant Current power supplying

To power our coil we have two options, we can either provide a **constant voltage** or a **constant current**.

Using a constant current source is not advisable due to the **heating problem** of the coil. At **high currents**, as the coil is run, it will **heat up** and **its resistance will increase which will induce the power source to increase the voltage supplied to keep the current constant**. This in turn will cause the coil to heat up even more and the cycle will continue until the coil is damaged. This is the phenomenon of thermal runaway we discussed before.

Instead, using a **constant voltage source** as the resistance increases due to the coil **exceeding the heating and power threshold we will only induce a decrease in the supplied current** which results in a loss of magnetic field strength but the coil won't get damaged.

2.4 Modelling of the Entire System

To be able to produce vibrations using the magnetic field produced by the coil we need to introduce to the system an object that can react to the magnetic field. As the magnetic field of the coil is very feeble we can use **Neodymium magnets**, these are permanent magnets with a very **strong internal magnetic field** for their size. With the right pole facing the coil (same polarity as the generated magnetic field) it will be able to **repel** them and make them vibrate. Then to constrain the motion of the magnet and make it only move in the z-axis we have to add to the system a **flexible membrane**.

The entire system can be modeled using a bond graph, as shown in figure 2.12.
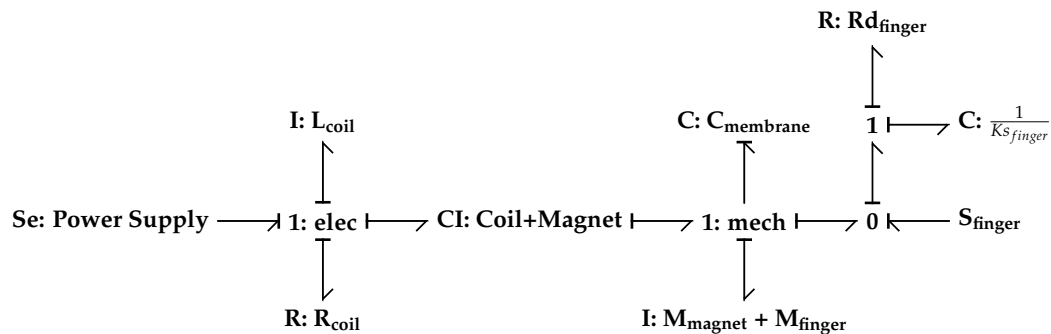
FIGURE 2.12: Complete bond graph of the entire system, describing the electrical, mechanical and haptic components.

In the next subsections, we will analyze the physical laws that govern the behavior of the system and how to model them to create this bond graph.

2.4.1 Neodynium magnets (magnetic strength wrt class and dimensions)

Neodymium magnets are a type of rare-earth magnet, they are the strongest type of permanent magnets made commercially. They are made of an alloy of neodymium, iron, and boron and their **strength depends on the percentage of neodymium** in the alloy and on its crystalline structure. They are classified based on their maximum energy product, which is the maximum amount of energy that can be stored in a magnet. Modern neodymium magnets start from N35 and go up to N52 (even N55), the higher the number the stronger their magnetic field.

Considering a cylindrical magnet with a radius R_M and a thickness t we can calculate the magnetic field generated by it at a distance z from a pole surface using the formula [7]:

$$B_M(z) = \frac{B_r}{2} \left(\frac{t + z}{\sqrt{R_M^2 + (z + t)^2}} - \frac{z}{\sqrt{R_M^2 + z^2}} \right) \tag{2.5}$$

Where:

- B_r is the remanence of the magnet [T]

- R_M is the radius of the magnet [m]

- t is the thickness of the magnet [m]

- z is the distance from a pole surface of the magnet [m]

The remanence of a magnet is the magnetic field that remains in the magnet after the external magnetic field is removed and depends on the N grade of the magnet.

Goudsmit Grade	Remanence $B_r\ [mT]$	
	min value	typical value
N35	1170	1210
N38	1220	1260
N40	1260	1290
N42	1290	1320
N45	1320	1370
N48	1370	1420
N50	1400	1460
N52	1420	1470

TABLE 2.2: Magnetic field remanence of different N grade neodymium magnets.

2.4.2 Magnetic force between magnet and coil

To calculate the magnetic repulsion force between the coil and a permanent magnet we consider them aligned with their centers coinciding on the z-axis.
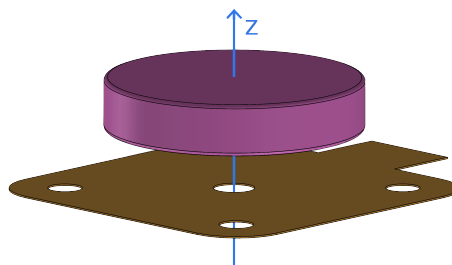

FIGURE 2.13: Coil and magnet position in space.

The force between a magnet and a coil can be calculated using the magnetic field generated by the two. Knowing their closed-form expression we can calculate the force using the equation for magnetic levitation between a permanent magnet and planar magnetic serpentines [8].

$$F = \nabla(\overrightarrow{m_M} \cdot \overrightarrow{B_C}) \tag{2.6}$$

Where:

- $\overrightarrow{m_M}$ is the magnetic moment of the magnet [A/m]

- $\overrightarrow{B_C}$ is the magnetic field generated by the coil [T]

The magnetic momentum of the magnet is defined as:

$$\overrightarrow{m_M} = \begin{pmatrix} 0 & 0 & \frac{B_M(z)}{\mu} \end{pmatrix}$$

Where:

- $B_M(z)$ is the magnetic field generated by the permanent magnet [T]

- μ is the magnetic permeability of the medium [H/m]

We can calculate the magnetic field generated by the coil at a distance using equation 2.4 (considering our coil as two in series) and the magnetic field generated by a cylindrical magnet at a distance z using equation 2.5.

Doing the calculations, the resulting force in function of the distance z is given by:

$$F = \frac{B_r I N R_C^2 \left(\frac{1}{\sqrt{\sigma_1}} - \frac{1}{\sqrt{\sigma_2}} + \frac{z^2}{\sigma_2^{3/2}} - \frac{2(t+z)^2}{2\sigma_1^{3/2}} \right)}{2\sigma_3^{3/2}} + B_C(I) \cdot \frac{3z \left(\frac{z}{\sqrt{\sigma_2}} - \frac{t+z}{\sqrt{\sigma_1}} \right)}{2\sigma_3}$$

Where:

- N is the number of spires of a one-layer coil

- I is the current flowing through the coil [A]

- B_C is the coil magnetic field calculated as in 2.4 [T]

- R_C is the coil average radius (r' in equation 2.4) [m]

- $\sigma_1 = R_M^2 + (t+z)^2$

- $\sigma_2 = R_M^2 + z^2$

- $\sigma_3 = R_C^2 + z^2$

So we can model the coil-magnet system as a **transducer** element that converts the current flowing through the coil into a force acting on the magnet.

$$B_C(z, I) = \frac{\mu N I R_C^2}{2(R_C^2 + z^2)^{\frac{3}{2}}} \rightarrow B_C(q, i) = \frac{1}{2}L(q)i$$

$$\vdash \xrightarrow[i]{V} \text{ CI: Coil+Magnet } \xleftarrow[V]{F} \dashv$$

$$F(q, i) = \frac{1}{2}\frac{d\left(L(q) \cdot m_M(q)\right)}{dq}i$$

$$\lambda = L(q)i$$

FIGURE 2.14: Coil-Magnet Transducer bond graph.

The last two equations represent the **standard notation for the constitutive equations** of the transducer element we described. The equation for the force (derived from 2.6) represents the relation between the **input flow** (the coil current i) and the **output effort** (the force F). Meanwhile, λ represents the **flux of the coil** which in this case is the **output flow** of the transducer.

2.4.3 Membrane-magnet system

The magnet needs to be **suspended** to allow it to move freely only on the **z-axis**. To achieve this we need a structure that **constrains** its **lateral motion** and also needs to be able to vibrate freely with it. To do this we can use a **flexible membrane** that can deform under the force generated by the interaction of the magnetic field of the coil and magnet.

As an example, we will analyze the membrane structure of the last implemented prototype 5.3.
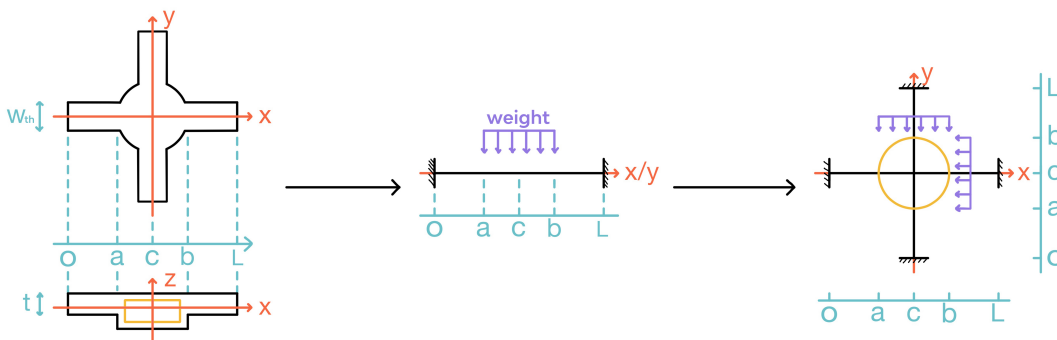

FIGURE 2.15: Membrane structure and mechanical two fixed beams
model of the last prototype.

This membrane is a simple **celtic-cross** structure made of thin **silicone** integrated with the entire structure of the device, the membrane is built with a central cylindrical chamber used to trap the **magnet in the center of the cross** as we can see in figure 2.16.
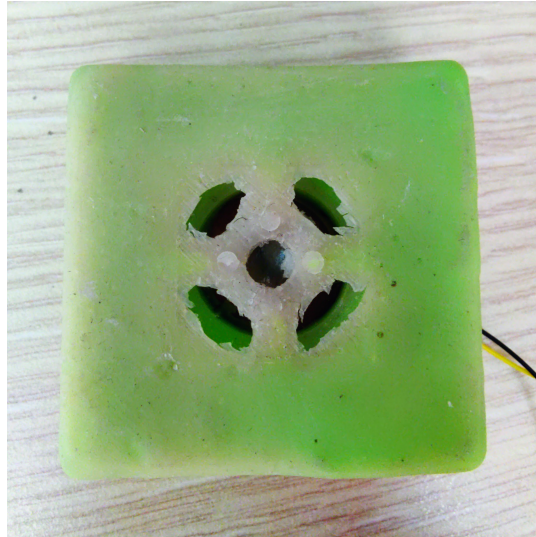

FIGURE 2.16: Membrane of the last prototype with the magnet trapped in the center.

The membrane can be modeled as a mass-spring-damper system.
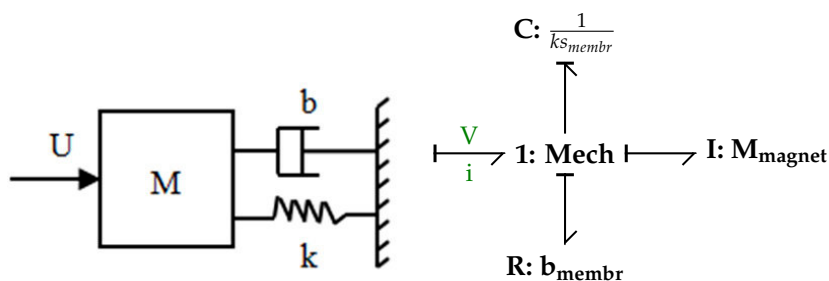
FIGURE 2.17: Bond graph of the membrane-magnet system.

Membrane stiffness

The membrane stiffness can be calculated using Young's modulus of the material, the geometry of the membrane and the load characteristics.

The geometry of the membrane can be modeled as two **fixed beams** perpendicular to each other and connected at the center (model in Figure 2.15). They are both under a shared **partially distributed load**, the magnet's weight.

Where we approximate the distribution of weight on the membrane as the weight of the magnet **distributed across its diameter**.

For each beam, the distributed load can be calculated as:

$$w = \frac{\frac{M_m}{2}g}{2r}$$

Where:

- w is the distributed load [N/m]

- M_m is the mass of the magnet [kg]

- g is the gravitational acceleration [m/s^2]

- r is the radius of the magnet [m]

We approximate by considering only **half** of the magnet's **weight** as we have **two beams supporting** the magnet.

Then the stiffness of a single beam is defined as:

$$ks = \frac{P}{\delta_{max}} = \frac{wr}{\delta_{max}}$$

Where:

- ks is the stiffness of the beam [N/m]

- P is the load on the beam [N]

- δ_{max} is the deflection of the beam [m]

Considering the structure shown in figure 2.15, the **maximum deflection** of a fixed beam under a distributed load can be calculated as:

$$\delta_{max} = -\frac{R_A c^3}{6EI} - \frac{M_A c^2}{2EI} + \frac{w(c-a)^4}{24EI} \tag{2.7}$$

Where:

- R_A is the reaction force at the origin of the beam [N]

- M_A is the moment at the origin of the beam [Nm]

- E is the Young's modulus of the material [Pa]

- I_x is the second moment of inertia of the beam on the x-axis [m^4]

- w is the distributed load [N/m]

- c is the distance between the origin of the beam and its center [m]

- a is the distance between the origin of the beam and the start of the distributed load [m]

We will only focus on the calculation of the **second moment of inertia** of the beam, the equations for the **other parameters** can be found in the reference [9].

The beam can be simplified as a parallelepiped with a rectangular section, and the second moment of inertia on x can be calculated as:

$$I_x = \frac{w_{th}t^3}{12} \tag{2.8}$$

Where:

- w_{th} is the width of the membrane arms as in figure 2.15[m]

- t is the thickness of the membrane as in figure 2.15[m]

Then we can consider the 2 beams as 2 springs in parallel, the total stiffness of the membrane can be calculated as:

$$ks_{membr} = 2ks$$

Membrane damping

The **damping** for a cantilever beam is **neglectable**, so we can remove the **resistive component** from the mechanical model.
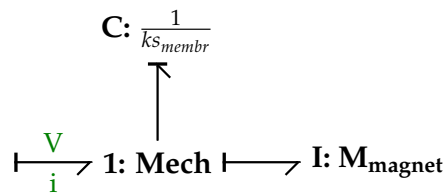

FIGURE 2.18: Final mechanical bond-graph of the membrane and magnet.

2.4.4 Finger grasping model

At last, we have also to model the **finger grasping** the device, we can derive the model from the one used in the paper [10] for the human finger.
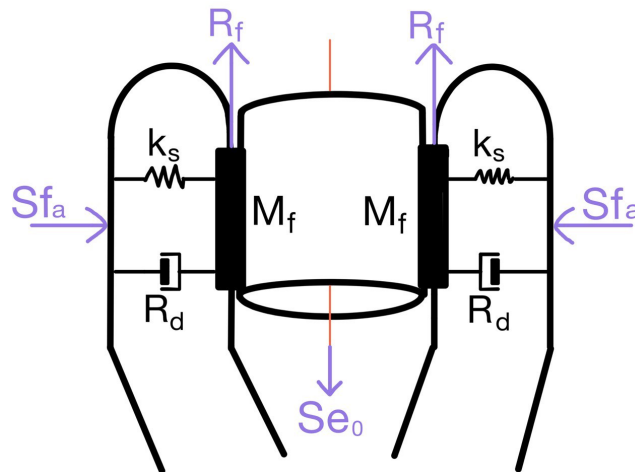

FIGURE 2.19: Model of two soft fingers grasping the object.

This model describes two fingers grasping an object, for our case, we can simplify it to a **single finger grasping** the device. Also, we can **neglect the friction** between the finger and the device as the device will be tested positioned on a flat surface with only the finger touching it from above.

$$\textbf{R: Rd}_\textbf{f}$$

$$\textbf{I: M}_\textbf{f} \qquad \textbf{1} \longmapsto \textbf{C: } \frac{1}{Ks_f}$$

$$\overset{\textcolor{green}{F}}{\underset{\textcolor{green}{v}}{\longrightarrow}} \textbf{1} \longmapsto \textbf{0} \longleftarrow \textbf{Sf}_\textbf{a}$$
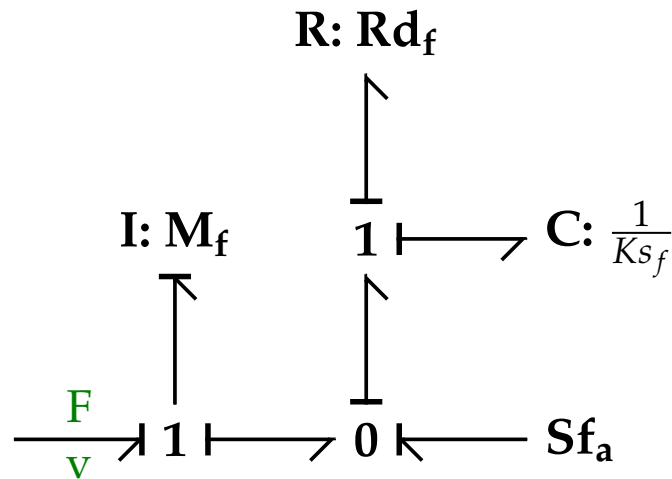
FIGURE 2.20: Bond graph of the finger grasping model.

The finger grasping can be modeled as a **mass-spring-damper** system, where the inertia component is represented by the finger's mass, while the spring and damper represent respectively the stiffness and damping effect of the finger's skin.

Human skin's properties have been studied by a team from the University École Centrale de Lyon, they found it has a stiffness constant ranging between **47.3 and 128.3 N/m**, and a damping coefficient between **0.08 and 0.121 Ns/m** [11]. The mass of the finger varies a lot depending on the finger's size.

Chapter 3

Overview of Haptic Feedback

Haptic Feedback or Haptics, in short, is the research field that deals with the need to be able to **digitalize the human sense of touch and reproduce it**. Despite the research done in this field since the mid-20th century, the technology is still in its infancy. The main reason for this is the **complexity of the human sense of touch** which we still don't understand fully. This, in turn, doesn't allow us to even approximately match the capabilities of the human sense of touch; but we can still use this infant technology to reproduce **simple sensations**. Simple sensation reproduction can still be used in many fields, from the **entertainment** industry to the **medical field**, from the **military** to the **automotive industry** to **convey information that we do not normally acquire via touch**, such as notifications and warnings related to particular events, guidance instructions, and even crude reproduction of textures. In this chapter, we will give an overview of the human sense of touch and the state of art technologies used to reproduce it.

3.1 Physics of Haptic Feedback

3.1.1 Biology of Haptic Sensing

The human tactile sensing system can **measure specific properties of materials**, such as temperature, texture, shape, force, fine-form features, mass distribution, friction, hardness and viscoelasticity, **through physical contact** between the human skin and the object. Even the **changing state of the interaction**, such as gravitational and inertial effects, can be perceived through the sense of touch. As the sensing system works through the skin, it doesn't rely on a localized sensory organ but behaves as a **distributed system**, also **different parts of the body have different thresholds of sensitivity**. For these reasons, it's difficult to treat a tactile signal as a well-defined quantity like visual and audio signals and its complex nature makes it **difficult to replicate** its functioning in science or engineering tasks.

The sense of touch is based on the somatosensory system, which is a **complex system of nerve endings and touch receptors** in the skin. The somatosensory system is composed of four main types of receptors:

- **Mechanoreceptors** - These are the most common type of tactile receptors in the skin. They are responsible for sensing **pressure**, **vibration**, **stretching**, and **brushing**.

- **Thermoreceptors** - These receptors are responsible for **sensing temperature** changes in the skin. There are two main types of thermoreceptors: warm receptors and cold receptors.

- **Nociceptors** - These receptors are responsible for **sensing pain and tissue damage**. They are activated by noxious stimuli, such as extreme temperatures, pressure, or chemicals.

- **Proprioceptors** - These receptors are responsible for **sensing the position and movement** of the body. They are located in the muscles, tendons, and joints, and provide feedback to the brain about the relative position between different parts of the body.

The **most important receptors for haptic feedback are the mechanoreceptors**, they react to mechanical stimuli by producing **signals in the form of streams of voltage pulses** at high frequencies, the stronger the stimuli, the higher the frequency of the pulses. When the cell adapts to the stimulus, the pulse frequency subsides to its normal rate. Considering the goal of this research we can **focus** on the **mechanoreceptors** that are responsible for **sensing pressure and vibration**, these are the **Pacinian corpuscles** and the **Meissner corpuscles**. The first ones are more sensible to **high-frequency** vibrations (200-550Hz), while the second ones are more for **low-frequency vibrations** (20-40Hz) [12].

3.1.2 Haptic sensitivity

As the mechanoreceptors are **enveloped in various skin layers**, their sensitivity to vibrations will not be infinite. The **strength of the sensation** will depend on the **frequency** and **amplitude of the vibration**.

Referring to the objective of this thesis, the **amplitude** of the vibration can be considered in **terms of the acceleration of the membrane-magnet system**.

Previous works [13] found that, for a **pulp contact area** ranging from **53 to 176.7 mm^2**, the threshold of detection of vibrations was between **0.1778 and 0.5623 m/s^2** (in the work specified as 105-115 dB (re 10^{-6}m/s^2)) for sinusoidal stimuli ranging from **100 to 250 Hz**. For frequencies close to **125Hz** the threshold should also **lower** as the finger pulp reaches its **resonance frequency** [14].

The study also highlights that the sensitivity depends on the **constant pressure force applied on the skin** in conjunction with the vibration. They found that under active pressing force, the sensitivity threshold decreases to 0.027-0.143 m/s^2 (in the work specified as 68.5-83.1 dB (re 10^{-6}m/s^2)) for a constant applied force of 1.6N.

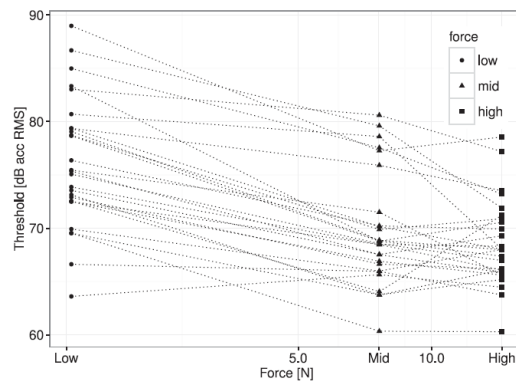For higher pressure forces the sensitivity threshold decreases even further, as we can observe in Fig. 3.1.

FIGURE 3.1: Pulp vibration sensitivity as a function of the applied pressure [14].

3.2 State of the Art in vibrotactile haptic feedback

For now, state of the art in haptic feedback is still in its infancy. The main reason for this is the complexity of the human sense of touch which we still don't understand fully. The **best technology** we have for now to reproduce haptic feedback through **vibrotactile** means is the **piezoelectric actuator**.

3.2.1 Piezoelectric actuators

Piezoelectric actuators are a very interesting technology based on the **piezoelectric effect**. Materials exhibiting this effect, such as certain ceramics and crystals, possess the ability to **convert electrical energy into mechanical motion**, and vice versa.

The operating principle of piezoelectric actuators relies on the application of an electric field across the piezoelectric material. This electric field induces a **deformation within the material**, causing it to expand or contract depending on the polarity of the applied voltage. This minute deformation translates into **highly precise mechanical displacement**, enabling piezoelectric actuators to achieve nanometer-scale resolutions with **remarkable speed and accuracy**.

One of the defining characteristics of piezoelectric actuators is their **rapid response time**. Unlike traditional electromagnetic actuators, which may suffer from inertia and mechanical backlash, piezoelectric actuators can swiftly change their state in response to electrical signals.

Frequency response

Piezoelectric actuators are perfect for haptic applications as they can provide a **wide range of frequencies**. Piezo specifically engineered for haptic feedback can provide a frequency range from 1 Hz to 1 kHz.

All piezoelectric actuators have a natural frequency at which they resonate. This **frequency** is determined by the **mechanical properties** of the actuator, such as its mass and stiffness, as well as the electrical properties of the piezoelectric material.

The important thing to note is that this **frequency also depends on the load** that the actuator is driving:

$$f_{res} = \frac{1}{2\pi} \sqrt{\frac{k}{m_{eff} + m_{load}}}$$

Where:

- f_{res} = Resonant frequency [Hz]

- k = Stiffness of the piezo actuator [N/m]

- m_{eff} = Effective mass of the actuator [kg]

- m_{load} = Mass of the load [kg]

As the frequency of the actuator approaches its resonant frequency, the **amplitude** of the actuator's motion **increases significantly**. This phenomenon must be taken into account when designing a control system for the piezo actuator, as at maximum voltage the actuator could be **damaged** if in resonance.

Force performances

Taking as an example a piezo actuator built specifically for haptic feedback, the PowerHap series from TDK [15], we can see that the actuator can provide a force up to **20N** in a frequency range from 1 Hz to 500Hz.

Power consumption

Considering still as an example the PowerHap series from TDK, we can read from the datasheet that the actuator can be run with a peak voltage of 120V and an average current of 0.432A (calculated using [16] in the case of a square wave signal of 500Hz). This means that the actuator can **consume** up to **25.9W** of power at its peak frequency. In the same condition, it will also **dissipate** about **2.59W** of power as heat.

Chapter 4

Powering circuit design

In this chapter, we will present some of the engineering challenges faced during the **design of a power circuit** for our flexible voice coil actuator. We will mostly describe an ideal circuit as we will later demonstrate that running this actuator would require very **advanced analog circuitry**, comprised of **high-cost components**. Most of the tests we will present have been done using a **laboratory bench signal generator and amplifier**.

4.1 Power Circuit Block diagram

To design the power circuit for the flexible voice coil actuator, we started by analyzing the requirements of the actuator. First of all, we want the coil to be driven with a sinusoidal **AC signal** at various frequencies and amplitudes; so the first component to consider it's the **system's controller** which in this case, can be a **simple signal generator**. For our application, we chose a simple **ESP32** microcontroller, which has an **integrated DAC**.

Then we have to consider the **power requirements** to run the chosen coil. The impedance of a Flexar coil, as we discussed before, is in the order of 30Ω. The impedance of the coil is **too low** to be driven directly by the ESP32 DAC, so a **power stage** is needed. For the sake of simplicity, we chose to implement a power stage with a **fixed gain** of 10.

Then we want the amplitude of the signal to be adjustable, so we needed a **conditioning circuit** to adjust the amplitude of the signal coming from the DAC **before being amplified**.

The control circuit can be summarized as a block diagram, as shown in figure 4.1.

FIGURE 4.1: Block diagram of the power circuit.

4.2 Controller

The controller in this application has to be a **signal generator** that can produce a waveform that can be amplified and sent to the coil. The controller we used for testing is an ESP32 microcontroller. We chose this controller as the first test hardware for its **simplicity of programming** and its **integrated DAC**.

4.2.1 ESP32 DAC Characteristics

The DAC included in the ESP32 is a pretty basic one but as a first test, it is enough. The DAC has a resolution of **8 bits**, and it can output a voltage between **0** and **3.3V** with a maximum current output of **12mA**.

4.2.2 ESP32 waveform generator

Using a simple program the ESP32 can be used as a pretty capable waveform generator. The software we used is the **ESP32 Signal Generator** from **corz.org** [17]. This software allows the user to generate the following waveforms:

- Sine wave from 16Hz to 500kHz

- Square wave from 1Hz to 40MHz

- Triangle wave from 153Hz to 150kHz

- Sawtooth wave from 153Hz to 150kHz

Between these ranges of frequencies, the generated waveforms are pretty accurate.

FIGURE 4.2: ESP32 16Hz Sine wave generated by the ESP32 Signal Generator software.

4.3 Signal Conditioning Circuit

We know that the controller DAC **outputs a voltage** between **0** and **3.3V**, the power stage has a **gain of 10**, and that to drive Flexar's coils, at their rated **maximum power of 0.8W**, we need to provide a voltage of about **6V** at a current of **0.2A**.
A very simple solution is to implement a **variable voltage divider** to adjust the amplitude of the signal coming from the DAC.
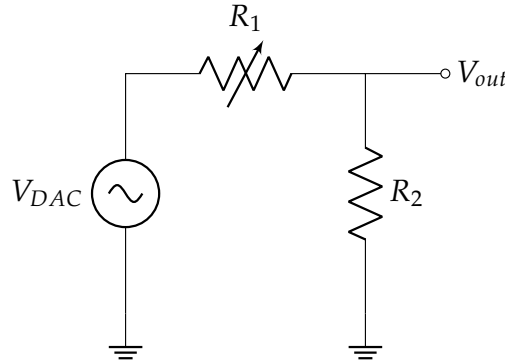
We chose a **maximum dividing factor of 10** to match the power stage gain.

FIGURE 4.3: Signal conditioning circuit.

Where:

- V_{DAC} is the voltage coming from the controller DAC [0,3.3]V.

- R_1 is a $100k\Omega$ potentiometer to adjust the amplitude of the signal.

- R_2 is a $10k\Omega$ resistor to set the maximum amplitude of the signal.

- V_{out} is the output voltage of the conditioning circuit [0, 0.33]V.

The output voltage of the conditioning circuit is given by the following formula:

$$V_{out} = V_{DAC} \cdot \frac{R_1}{R_1 + R_2}$$

The values of R_1 and R_2 have been chosen to be $100k\Omega$ and $10k\Omega$ respectively, as they are standard values, provide a good range of adjustment for the amplitude of the signal, and their order is **big enough** to work with the provided DAC current of 12mA.

4.4 Amplifier circuit

As the Flexar's coil impedance is 30Ω, and the maximum power they can withstand is 0.8W, the power stage must be able to provide a voltage of about **6V** at a current of **0.2A**.
Such a high current requires the use of a power amplifier, usually an off-the-shelf audio amplifier could be used in such an application. Such devices are built to handle only the **audible frequency range** (20Hz-20kHz), but our actuators must be able to work between **1Hz and 1kHz** which corresponds to the **human tactile perception range**.

A solution is to implement a custom amplifying circuit based on a special type of operational amplifier, the Power OP-AMP.

4.4.1 Power Operational Amplifiers

Power operational amplifiers (power op-amps) are a specialized class of operational amplifiers designed to handle **higher current** and **power requirements** than standard op-amps. While traditional op-amps are primarily used for signal processing and conditioning in low-power applications, power op-amps are essential for **driving heavy loads**, including motors, speakers, and other devices that require substantial power.

Power op-amps integrate the fundamental principles of conventional op-amps such as high gain, high input impedance, and low output impedance with the ability to deliver higher current and power.

These devices are composed of simple op-amp circuits with a **power stage**, usually a **power transistor**, connected to the output of the op-amp. The power stage is responsible for delivering the required current to the load, while the op-amp provides the necessary voltage gain and feedback control.
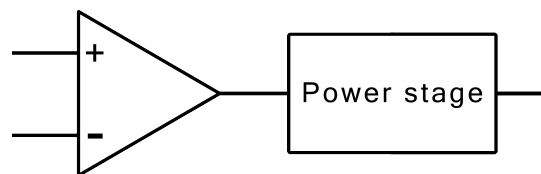
FIGURE 4.4: Power Op Amp block diagram.

Power op-amp characteristics

Any op-amp that can deliver **more than 100mA** of current is considered a power op-amp; there exist models that can deliver up to **10A**. For our application, we chose a power op-amp that can deliver up to **1A** of current, as it is more than enough to drive the Flexar's coils for simple AC signals. Another factor for this decision is the **high cost** of these components, especially at higher current ratings, due to their **complexity** and the **scarcity of requests** for this type of component from the market.

The component we landed on is the **L272** from STMicroelectronics, this small chip can deliver up to a **sustained 1A** of current, **1.5A** of **peak** current, and can handle a **maximum supply** voltage of **28V**.

In dynamic conditions is also to be noted that the L272 has a **slew rate of** $1\frac{V}{\mu s}$ and, a **gain-bandwidth product** of **350kHz** [18].

Power dissipation problems

A big problem with power op-amps is the **power dissipation**, as they are designed to deliver high current levels, they also dissipate a lot of power, which can lead to **overheating** and damage to the device.
For example, the L272 can handle up to **145°C** but at only **5W** it reaches **75°C**, so a **heat sink** is required to keep the device at a safe temperature.

4.4.2 High Power Voltage Amplifier

As we specified before we decided to implement a power stage with a gain of 10, starting with the circuit of a simple **inverting amplifier** (the real gain is -10 but for the sake of our application a wave flipped by 180° is acceptable).
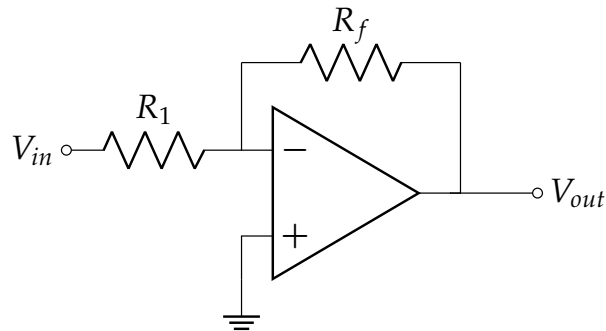

FIGURE 4.5: Inverting amplifier circuit.

The gain can be calculated using the following formula:

$$A = \frac{V_{out}}{V_{in}} = -\frac{R_f}{R_1}$$

Where:

- V_{in} is the input voltage.
- V_{out} is the output voltage.
- R_1 is the input resistor.
- R_f is the feedback resistor.

The values of R_1 and R_f have been chosen to be $4.7k\Omega$ and $47k\Omega$ respectively, as they are **standard values** and their order is **big enough** to work with the provided DAC current of **12mA**.

4.4.3 Noise filtering

While implementing the amplifier circuit, we noticed that the output signal had a lot of **high-frequency noise**, which was not present in the input signal.

To solve this problem, we decided to implement a simple **low-pass filter** adding a capacitor in parallel with the feedback resistor.
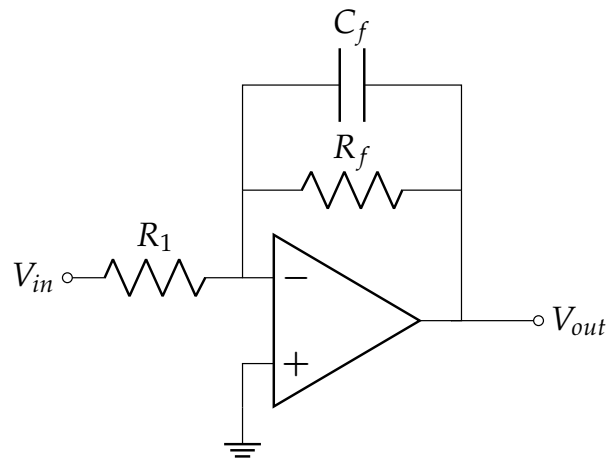
FIGURE 4.6: Inverting amplifier circuit with the low-pass filter.

The cutoff frequency of the filter can be calculated using the following formula:

$$f_c = \frac{1}{2\pi R_f C_f}$$

Where:

- f_c is the cutoff frequency [Hz].

- R_f is the feedback resistor [*Omega*].

- C_f is the capacitor in parallel with the feedback resistor [F].

We set a **cutoff frequency** of **50kHz**, as it is high enough to filter out the noise but low enough to keep the signal intact. To achieve this, we chose a capacitor of **680pF**, as it is a standard value and provides a cutoff frequency of 50kHz with the chosen feedback resistor.
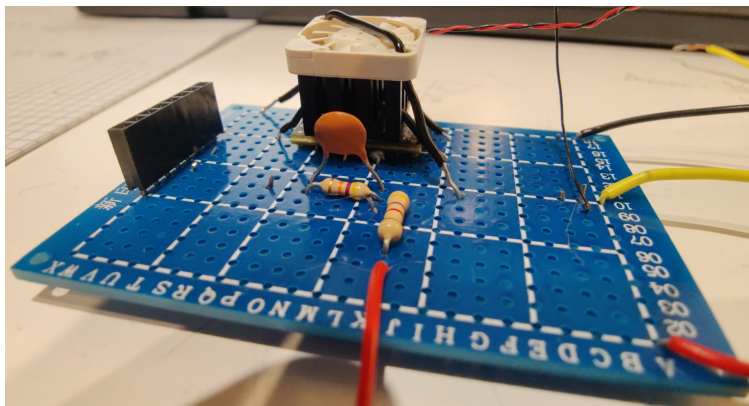
FIGURE 4.7: Picture of the implemented power stage.

Chapter 5

Implementation and Prototypes

5.1 Coils alternatives

This research was originally born from the willingness to explore the possibility of exploiting the technology of flexible coil inductors by using one produced by the research group **Helmholtz-Zentrum Dresden-Rossendorf** (HZDR) in Dresden, Germany [19]. After testing this coil, we realized its **limitations** and decided to explore other alternatives.

For our research, we landed on **Flexar coils**, which as we discussed before are flexible PCB coils produced by the company **microbots** [20]. In this section, we will compare Dresden coils with Flexar ones.

5.1.1 Dresda coils

The technology the HZDR team used to produce their coil is based on **circuit inkjet printing**. Circuit inkjet printing consists of using a printer to **deposit conductive ink** on a substrate. In this application, they used a **flexible substrate** to print the coil to allow it to be bent.

After printing the conductive ink is **tinned** to improve the conductivity of the coil and allow it to be soldered to other components.

FIGURE 5.1: Dresden coil [19].

Low resistance and high power needs

The Dresden coils have a resistance of about 2Ω, the external radius of $5 \cdot 10^{-3}$**m**, the internal one of $0.84 \cdot 10^{-3}$**m**, and the number of spires equal to **11**. We also know from the HZDR test that the coil can handle up to about **500mA** before starting to release too much heat. This means a power limit of about **0.5W** for the coil.

The current limit is due to the **very low resistance** of the coil as for low applied voltages the coil will produce a lot of heat due to the **Joule effect** 2.3.2.
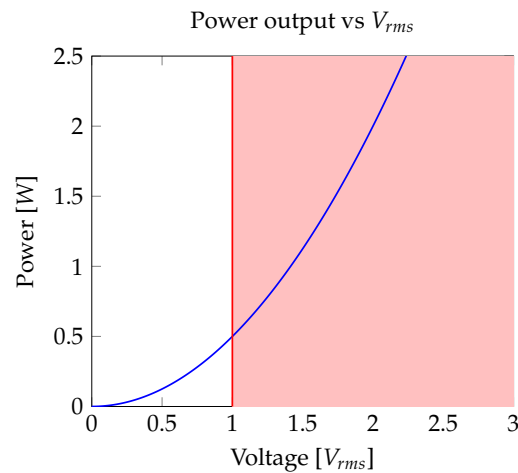
FIGURE 5.2: Power profile of the Dresden coil

As we can see in figure 5.2, after 1V the power limit is already reached.

Low magnetic field strength

For the same reason as the power limit, the magnetic field produced by the Dresden coil is **very low**. Using the equation 2.3 we can calculate the magnetic field produced by the Dresden coil on its surface and plot it as a function of the voltage applied to the coil (Fig. 5.3).
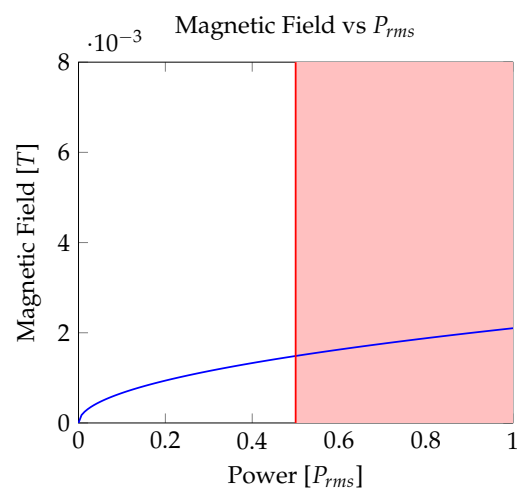
FIGURE 5.3: Magnetic field produced by the Dresden coil

As we can see in figure 5.3, even at the power limit, the magnetic field produced by the Dresden coil is very low (in the order of 1mT).

Fragility and low flexibility

The Dresden coil is produced by using **three layers** of different materials. The first layer is the substrate, which is made of a material similar to **paper**, the second layer is the **conductive ink**, and the third layer is the **tinning**. The substrate is **not very flexible**, and neither is the tinning; this makes the spires of the coil **easily damageable if bent repeatedly**. Also, the tinning gets **cracked** by repeatedly heating and cooling the coil, which constantly happens during the coil's use. The tinning cracking would happen multiple times during our tests, and we would have to **re-tin the damaged parts** of the coil to keep using it.

5.1.2 Flexar coils

Flexar coils are flexible PCB coils designed by the independent researcher **Carl Bugeja** [21]. He designed these very thin flexible coils intending to use them to actuate very **small robots** and **lightweight objects**. This characteristic comes at the cost of not being able to produce very high magnetic fields. We will be using for this research an old model of the Flexar coil that precedes the opening of the company **microbots** [20].
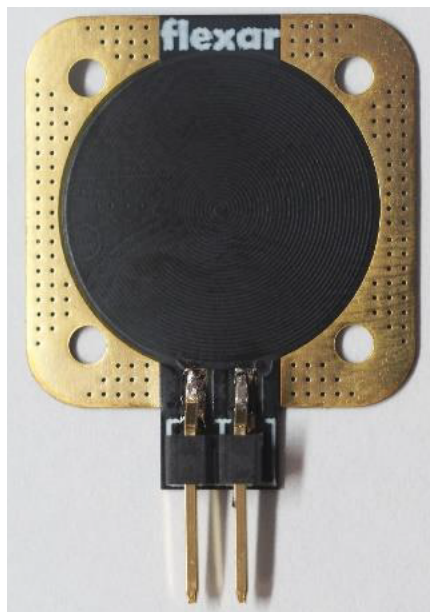
FIGURE 5.4: Flexar coil

Lower resistance and power needs

We previously discussed the Flexar coil's characteristics in section 2.3.2. But to sum up they have a resistance of about **30Ω**, external radius of $6.86 \cdot 10^{-3}$**m**, internal one of about 10^{-4}**m**, and number of spires equal to **70** (composed of two coils of 35 in series).

It can handle up to about **0.8W** before starting to release too much heat.

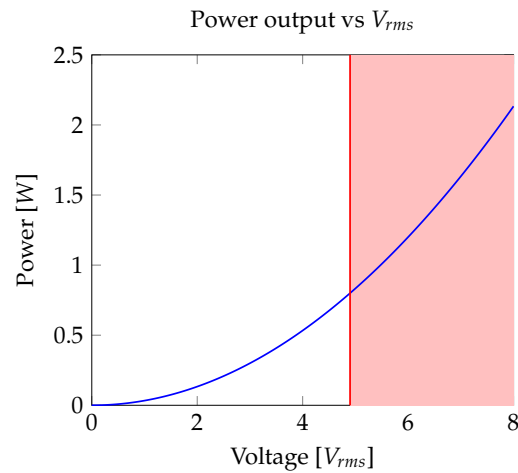We report here the same graph as the previously cited section:

FIGURE 5.5: Power profile of the Flexar coil

As we can see in figure 5.5, the Flexar coil can handle more power than the Dresden coil.

Higher magnetic field strength

Due to their characteristics, Flexar coils can produce **higher magnetic fields** than the Dresden coil but not unlike them, they are **still limited** by the power they can handle.
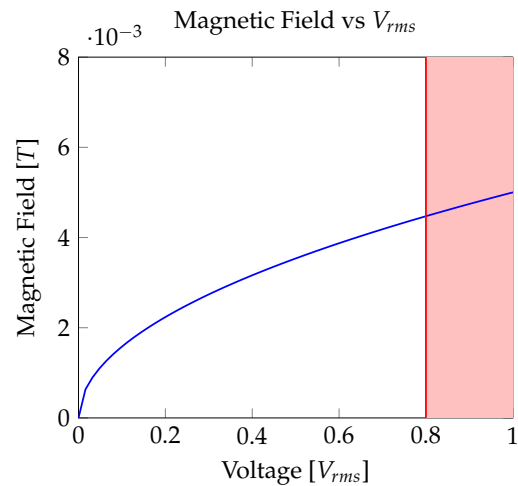

FIGURE 5.6: Magnetic field produced by the Flexar coil

As we can observe in figure 5.6, the Flexar coil, at the power limit of the Dresden coil, can produce a **higher magnetic field** (in the order of **2.5mT**). This proves that the Flexar coil is **more capable** than the Dresden coil in producing magnetic fields but even at its power limit, the field produced is **still feeble** (it is in the order of **(4mT)**).

Higher flexibility

Flexible PCBs are made of a substrate of **polyimide**, which is a **very flexible material**. It can withstand being bent at a very tight radius **multiple times without breaking**.

Between the layers of polyimide, we have the **copper traces** that don't require any tinning to work. This makes the Flexar coil **more durable** than the Dresden coil, as it doesn't have any parts that can crack due to bending or heating and cooling.

Also, we observed that the Flexar coil can withstand temperatures in exceed of **100°C**.

5.2 Rigid Prototypes

The goal of this research is to develop a flexible device, but before delving into flexible prototypes we started by designing some rigid ones. The rigid prototypes were designed to test the concept of this device and to understand the **limitations** of the technology.

5.2.1 1st version - Dresda Coils testbed

The first prototype was designed to test the capabilities of the Dresden coils. In the previous research done by the HZDR team [19] they tested the coil using a simple piece of **flexible magnetic tape as a membrane**.

Flexible magnetic membrane

This membrane is shaped like a "fish" so the tail can be fixed on a plane and the head can be **free to bend** up and down (as seen in Fig.5.7).
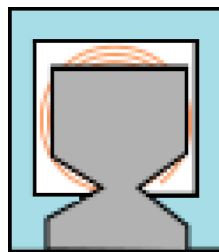

FIGURE 5.7: Dresden coil HZDR test setup

When the coil is powered, the magnetic field produced by the coil repels the membrane and bends it up. The coil would be powered with an **AC signal** at various frequencies, then one would need to keep his pulp **suspended** at a certain distance over the membrane and feel the vibration produced by the membrane. The pulp needed to be suspended at a certain distance to **avoid pressing** on the membrane, this would have caused the membrane to **stop vibrating**.

Adjustable height platform for coil and membrane

The most important thing to solve was to find a way to keep the pulp at a certain distance from the membrane.

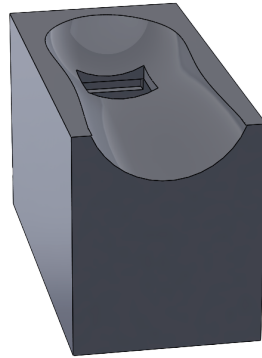Firstly we designed a platform that could keep the finger steady.

FIGURE 5.8: Finger platform

This platform was modeled to have an **ergonomic** cavity for the finger to rest in and a hole for the pulp to be suspended over the membrane. The square hole is large enough to allow the "fish" membrane to move **freely**. Under the hole, there is a large cavity where a mechanism is placed. This mechanism is a platform where the coil and membrane can be placed in a configuration similar to the one used in the HZDR experiment. The platform can then be **raised or lowered** to find the right distance between the membrane and the finger pulp.
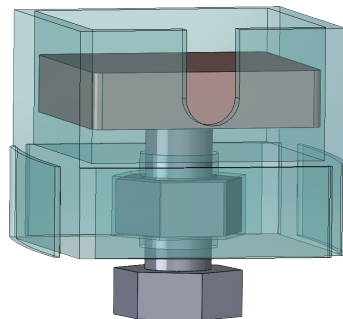
FIGURE 5.9: Adjustable platform

The mechanism is a simple screw that can be turned to raise or lower the platform, which is laying on top of it.

Prototype usability

This prototype proved to be pretty **difficult** to use. The main problem was that distance couldn't be easily adjusted as the platform wouldn't remain **stable enough** on the screw. This meant that finding an optimal distance between the pulp and the membrane was difficult, especially because different people have **different pulp thicknesses**. Even if a distance that was good for one person was found, the vibration produced by the membrane was **very weak** and could barely be felt.

5.2.2 Wearable Rigid Prototypes

With this prototype, we wanted to try **fixing most of the problems** encountered with the previous prototype.

Firstly we decided to substitute the Dresden coil with the Flexar one as it was more powerful. Then we wanted to **decouple the membrane** from the coil to prevent the membrane from being pressed by the pulp and remove the need for an adjustable platform to keep the coil at the right distance. Finally, we wanted to make the device **wearable**.

Finger-Membrane interface

After some testing, we found that a good way to decouple the membrane from the coil and better the transmission of vibrations to the finger was to use a small **high-performance magnet** attached directly to the finger pulp.

For our testing, we used an **N42-grade** neodymium cylindrical magnet with a diameter of **10mm** and a height of **3mm**. This magnet was **fixed** to the index pulp of the tester using some non-toxic glue and then he would be able to feel substantial vibrations by moving his pulp closer to the powered-on coil (with an AC signal).

Considering this knowledge, we designed a **silicon sleeve** that could be **worn** on the finger, this sleeve has a cavity for the magnet to be inserted into and be kept **near the skin**.
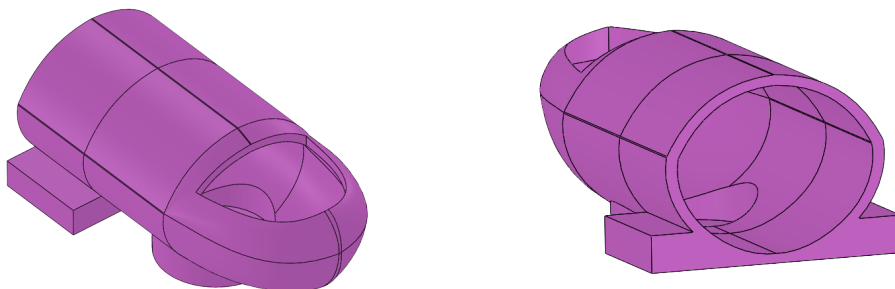
FIGURE 5.10: Finger silicon sleeve front and back view

This silicon sleeve was designed to be **scalable** for different finger sizes and to be easily worn and removed.

The design is composed of three parts:

- **Silicon sleeve:** This part was modeled by us on the profile of a real **3d scanned index finger**, it can be automatically scaled by specifying the index's width as all the measurements are based on that value.

- **Magnet hole:** The hole is designed based on the diameter of the magnet and its height. We also had to find the right **height tolerance** between the magnet and the pulp to avoid that it could press on the finger too much, impeding vibrations.

- **Mounting wings:** On the sides of the sleeve we have two parallelepipedal wings that are used to **mount the sleeve** to the structure where the coil will be attached (described in the following section).

Another design problem to solve was the **positioning** of the magnet, as the design had the goal of being adaptable to different fingertip sizes, we had to consider multiple finger widths. For the magnet position we chose the center to be placed on the **symmetry axis** of the pulp, then we based the design on index fingers with widths between **13mm** and **20mm** [22]. That meant that for 13mm fingers, the magnet size (10mm) was barely smaller than the finger's width, so knowing that the finger tends to get even narrower toward the tip, we had to place the magnet center closer to the **first interphalangeal fold** rather than to the pulp's center.
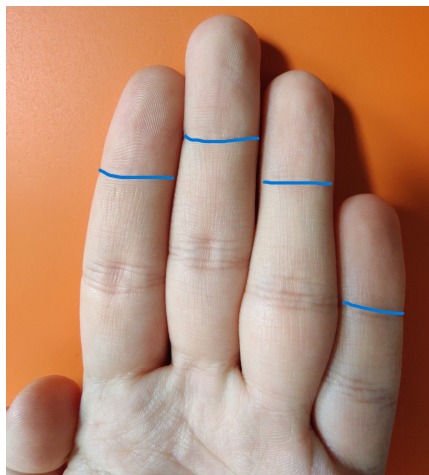

FIGURE 5.11: In blue we highlighted the first interphalangeal fold for each finger.

Sleeve production

The sleeve was produced by **silicon casting** inside a two-part 3D printed mold:

- **Mold cavity:** The cavity was designed based on the 3D model of an index finger, with the addition of a small surface to produce an opening at the fingernail (the part in grey in figure 5.12) and half of the hole necessary to create the magnet cavity.
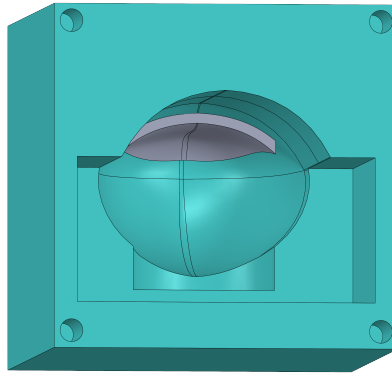
FIGURE 5.12: Mold cavity

- **Mold core:** The core was designed to be the negative of the cavity, including a part to create the other half of the magnet cavity and mounting wings (the part in light blue in figure 5.13). The negative is scaled down a bit to create a **casting clearance** of about **0.8mm**. This part also includes a cap that is screwed on the cavity to keep the core **suspended** in the silicon.
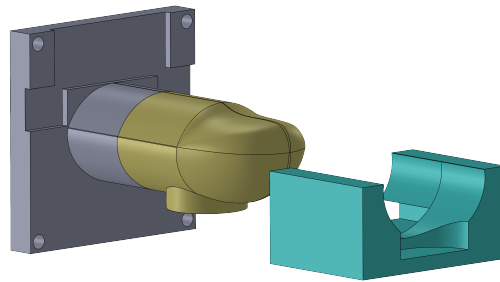

FIGURE 5.13: Exploded view of the mold core

The part went through multiple iterations to land on the **right thicknesses for the sleeve itself**, it needed to be thin enough to be **adaptable** to multiple fingers (considering similar widths) but not so thin as to be **durable** enough.

The material used for the casting was a **two-component silicon rubber** from ResChimica. We tested two different types of silicon, one with a **shore hardness** of **12** [23] and one with a shore hardness of **35** [24].

From our tests, we found that the silicon with a shore hardness of **35** was **too rigid** and **absorbed too much vibration** so we decided to use the softer one. The only problem with this softer silicon was its minimum curing time of **3 hours** at room temperature which always had to be increased as it never cured completely in that time.

Magnet-coil distancing structure

We then focused on a structure able to keep the coil at a **fixed distance** from the silicon sleeve and magnet. The design goals for this device were that it should be lightweight, easily wearable and adaptable to multiple sleeves' sizes.

After multiple iterations, we landed on a three-component design.

- **Sleeve holder:** This component (represented in Fig. 5.14) is the structure where the sleeve can be attached, this is done by inserting the mounting wings inside the two squared holes on the bottom of the part. The circle hole at the center of the component is where the magnet cavity of the sleeve with the magnet inside will be placed. The arch on the component front is present to allow the tip of the finger to support the weight of the structure.
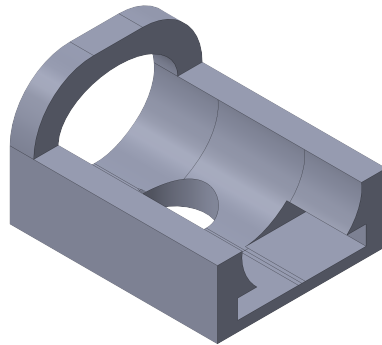
FIGURE 5.14: Silicon finger sleeve holder

- **Coil trap:** This component is the structure where the coil is inserted. This component is composed of 3 parts, a heatsink, a coil holder and a mask to screw the heatsink to the sleeve holder. The coil is sandwiched between the heatsink (the part in bronze in Fig. 5.15) and the coil holder (the part in grey in Fig. 5.15).

  Then they are screwed together to the sleeve holder.
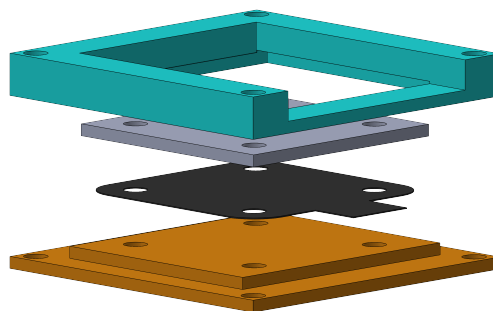
FIGURE 5.15: Explode of the coil trap

Heat dissipation

As the coil while active produces a lot of **heat**, we decided to introduce a **heatsink** in the design (the part in bronze in figure 5.15). The heatsink was made by cutting two small strips from a thin sheet of **copper** (**1mm** thick) that are joined together by **thermal paste** and screws. The same screws are also used to keep in place the coil and the coil holder.

For the same heat dissipation reason, we printed all components in **ABS** as it has a higher melting point than PLA.

Prototype usability

This prototype was much more usable than the previous one. The magnet was also kept at the right distance from the coil and the vibrations were **much more noticeable**, also being **wearable** made it much easier to use. The biggest problem of this prototype was the silicon sleeve, as the silicon tends to **absorb** some of the vibrations produced by the coil and the softness of the material made the **mounting mechanism** a bit **unreliable**. We also had to add a small **blowing fan** and another part to the heatsink (as we can see in figure 5.16) to keep the coil cool as it would **heat a lot** after a few minutes of use.
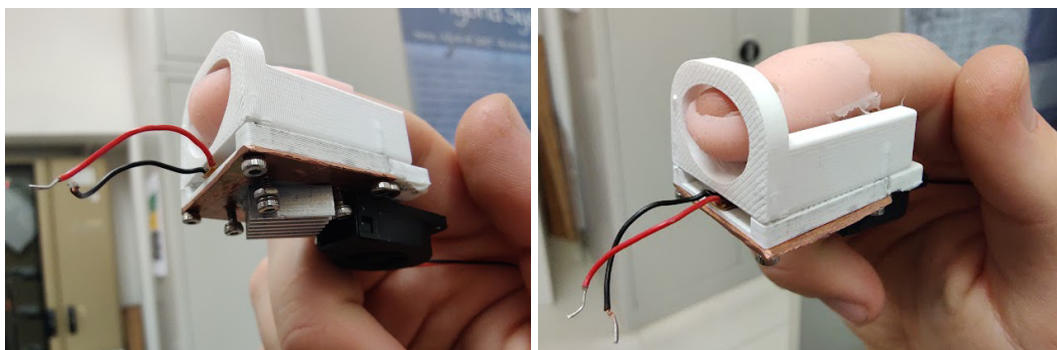
FIGURE 5.16: Bottom and top view of the real prototype

5.3 Flexible Mat Prototypes

The goal of these prototypes was to create a small silicone mat where the magnet could be suspended in a membrane **integrated into the mat** itself. **The coil and its heatsink would also be "trapped" inside the mat.** As the mat would be made of silicone, it would allow the device to **flex** with the flexible coil. As we **can't 3D print silicone** we had to create the entire design to be able to make it by **silicone casting** taking into account all the design limitations of this method. All the pieces were designed in SolidWorks and then 3D printed to create the molds for the silicone casting.

5.3.1 Design of the membrane

The design goal for the membrane was to create a structure that could support the magnet **just enough** to win over its gravitational force so that any other force applied to it on the z-axis would be enough to move it and make it vibrate. For the membrane design, we decided to use a simple Celtic-cross structure as we described previously in section 2.4.3. This resulted in a membrane with a central cylindrical chamber used to trap the magnet which is **suspended** by four parallelepipedal arms.
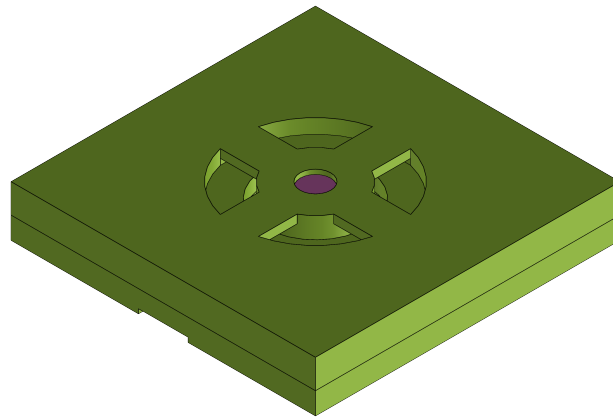
FIGURE 5.17: Membrane top view of the small magnet prototype.

Material stiffness and thickness

While prototyping we experimented with the same two different silicone materials we described in section 5.2.2. We quickly realized that the softer silicone was **too forgiving** as the membrane arms would need to be too thick to support the magnet. We so decided to move forward with only the **harder silicone** which allowed us to create thinner arms.

Membrane structure vs magnet dimensions

The main prototypes we realized were designed with two different N52 cylindrical magnets in mind. The first one is a small **10mm** diameter and **2mm** thick magnet, the second one is a **15mm** diameter and **3mm** thick magnet. The two magnets also have very different weights, the small one weighs **1.13g** while the big one **4.03g**. The first design of the membrane was based on the small magnet, thanks to it being lightweight it could be supported by a membrane with very thin arms(**0.6mm**) and a width of **4mm**. The membrane arms needed also to be long enough to allow the magnet to move freely on the z-axis, so we decided to make them **4mm** long.

FIGURE 5.18: Membrane cross-section of the small magnet prototype (t->thickness, L->length).

Switching to the big magnet we realized that the membrane arms would need to be **thicker** to support the magnet, even if we made them wider (**5mm**). This was due to

the increased weight of the magnet and the increase in the arms' length (now **5mm**) we needed to make to allow the magnet to move. To find the new necessary **minimal thickness** we used the model described in subsection 2.4.3. We set a **maximum deflection** of **0.8mm** for the membrane arms and calculated the thickness needed to support the magnet using equations 2.7 and 2.8. The results showed that the membrane arms would need to be at least **1.45mm** thick to support the magnet, so we decided to make them **1.6mm** thick to have a **safety margin**.

The next problem we encountered arose when we observed that the membrane arms were **breaking** at the connection with the cylindrical chamber. This was due to the **abrupt change of profile** that was causing a stress concentration at that point. To solve this problem we decided to add a **small fillet** to the connection between the arms and the chamber.
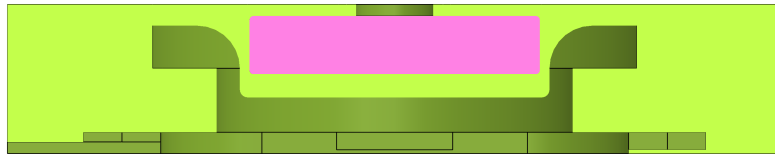
FIGURE 5.19: Membrane cross-section of the big magnet prototype.

5.3.2 Design of the mat

The mat structure is based on a simple idea but its design was **quite complex to be realized with silicon casting**. This is mostly due to our goal of integrating the membrane into the mat itself. This is due to our design goals:

- The membrane and magnet need to be **integrated into the mat** structure.

- There needs to be a mechanical way to keep the **coil** and its **heatsink steady** inside the silicone structure of the mat, as nothing can be glued to silicone.

- We need to create a **channel** for the magnet chamber to move freely on the z-axis.

- The complete structure must be able to **flex** somewhat.

As the silicon sleeve of the previous prototype 5.2.2 we opted for a **two-part mold** to create the mat:

- **Mold cavity:** The cavity was designed as a **parallelepipedal** empty box to create a simple external structure for the mat.
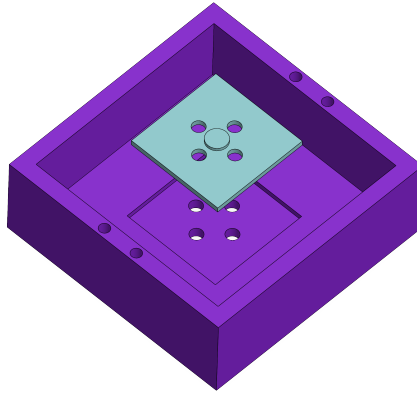

FIGURE 5.20: Flexible mat mold cavity

The purple component in figure 5.20 has four screw holes at the top to screw the **suspended core** to the cavity. The cavity also has a rectangular hole at the bottom where the small component in light blue is inserted. This component function is to work as a **pedestal** for the magnet, its exact function will be explained in the next section.

Through both components are carved four holes, these are used to allow the **excess silicone** of the casting process to **flow out** of the cavity.

The purple part needs to be 3D-printed in a flexible material to allow the mat to be **easily removed** from the cavity, in our case we used **TPU**.

- **Mold core:** The core is composed of multiple components that are inserted into the cavity to create the internal structure of the mat.

   In figure 5.21 we can see all the components of the core, which are:

   - **Mold core center** (in light blue) **:** This is the central component of the core, it is used to create the **coil membrane** and the **channel** for the magnet chamber to move.

   - **Coil trap** (in red) **:** This is the structure that will house the **coil** and its **heatsink** and the only part of the core that will remain inside the mat.

   - **Mold core cap** (in yellow) **:** This component is used to **keep the coil trap in place** and to prevent the silicone from **entering the coil trap**.

   - **Mold core - cavity bridge** (in pink) **:** This part screws into the core and the cavity to keep the core **suspended** in the cavity.

(A) Exploded top view of the mold core.

(B) Exploded bottom view of the mold core.

(C) Assembled top view of the mold core.

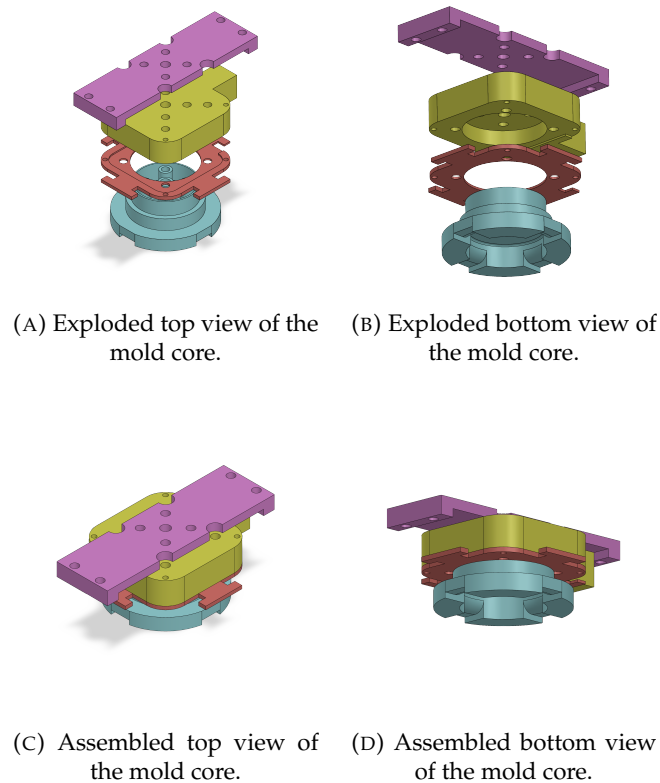(D) Assembled bottom view of the mold core.

FIGURE 5.21: Assembly of the mold core

Magnet chamber and membrane

To create the membrane and trap the magnet inside its chamber we needed a way to allow the silicone to **flow all around** the magnet.
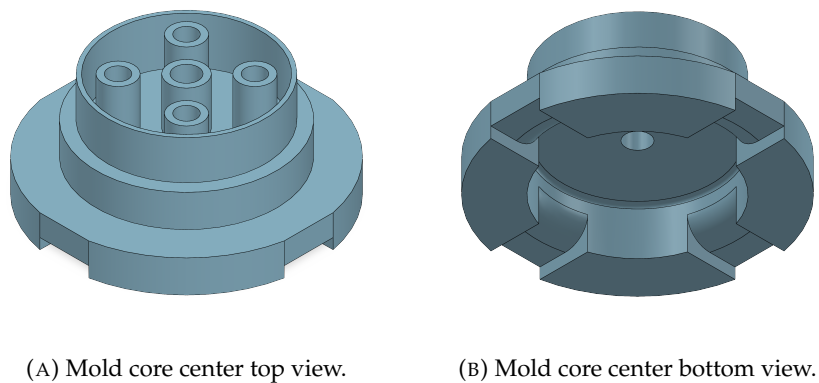

(A) Mold core center top view.

(B) Mold core center bottom view.

FIGURE 5.22: Mold core center.

To create the upper part of the chamber we modeled the mold core center to have a cylindrical hole in its center, deep and large enough to create a **silicone wall around the magnet** with a lateral thickness of **0.5mm** and a bottom thickness of **1.2mm**.

To cast the upper part of the chamber we created a **pedestal** (the light blue component in figure 5.20) for the magnet to rest on, the pedestal is a simple rectangular structure with a small circular bump at its center where the magnet is **glued**

on. When the silicone is set the pedestal can be **removed** and the magnet will be trapped inside the chamber by an **upper silicone ceiling** of thickness **0.6mm**. The **curved parts** and the **square holes** we can see in figure 5.22 are used to create the **membrane arms**.

The part used to create the channel is composed of three **different-sized cylinders**, the **first one** (the largest) is used to create the **space for the membrane arms to flex**, the **second one** is used to create the **channel itself** and the **third one** is used as a **support** for the coil trap and cap to **embed** them.

On the top, the center component presents four holes that are used to **screw it** onto the cap and one **larger central one** that reaches through up to the **magnet surface** which is used to pour the silicone into the chamber.

When the silicone is set the core center would remain **stuck into the mat** as it is too complex to be removed without damaging the mat itself. To solve this problem we decided to create the core center in a material that could be easily **dissolved** in water. This material is called **BVOH** and is a **water-soluble** filament that can be used as a support material for 3D printing. To speed up the **dissolution process** we decided to print the core center with **low infill** and shave some material off the smallest cylinder to allow the water to reach the BVOH more easily.

Distance magnet-coil

The middle cylinder is what dictates the **distance** between the **magnet** and the **coil**. This distance is crucial as it will determine the **strength of the magnetic field** that will reach the magnet. After multiple prototypes, we landed on a distance of **3.5mm** between the magnet and the coil. In theory, the distance could be lower but we had to take into account the **flexing of the membrane due to the pressure** on it generated by the finger grasping the device.

Coil trap

This component has two functions, the first one is to **house the coil** and its heatsink and the second one is to **trap the coil** mechanically inside the mat. Our main design limitations were that we **couldn't glue** the trap to the mat and that the trap needed to be able to **flex** with the mat and coil.
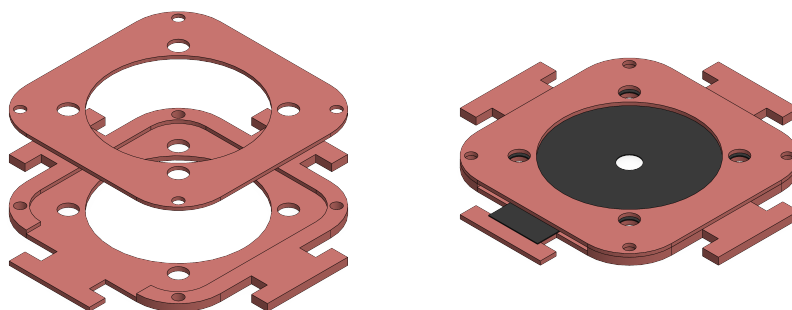
(A) Coil trap exploded view. (B) Coil trap with coil closed view.

FIGURE 5.23: Coil trap model.

The design we came up its a thin **square structure** with a small higher **border** where the coil is positioned (the lower part in figure 5.23). The coil is then covered by a **thin square plate** that is screwed to the trap (the higher part in figure 5.23). On the side of this square, we have four **thin fins** that will **remain inside the silicone structure** of the mat, mechanically **blocking the trap inside**.
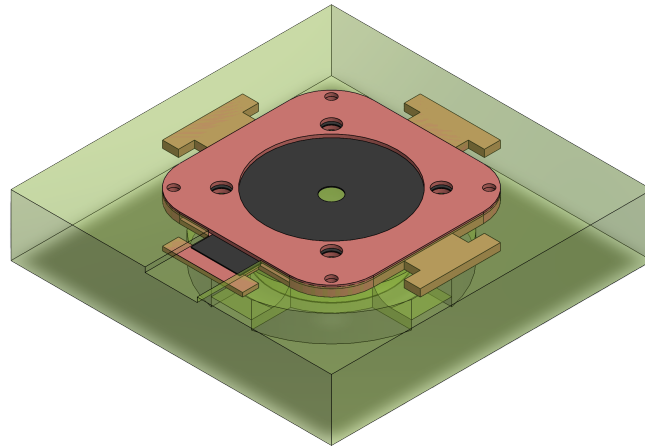
FIGURE 5.24: Coil trap placed inside the mat.

As the coil trap is very thin and it's printed in **TPU** it can easily **flex with the mat and the coil**.

Production method

To create a new mat various steps need to be followed:

- **Components printing:** All the components of the core and the cavity need to be printed.

- **Cavity assembling:** We first need to **glue the magnet to the pedestal** and then place it inside the hole at the bottom of the big part.

- **Core assembling:** We start by placing the bottom part of the coil trap on the smallest cylinder of the core center, then we screw the mold core cap and bridge to the core center and finally we screw the bridge to the cavity.

- **Silicone casting:** We **mix the silicone** and **pour it** first into the **big hole on top of the cap** with a syringe until the chamber is filled, we can notice when it's full by observing the **holes at the bottom of the cavity** and the membrane holes on the core center. We then pour the rest of the silicone into the cavity until the silicone **covers the coil trap fins**.

- **Removing the mat from the mold:** After the silicone is set we can remove the mat from the mold by unscrewing the bridge and pulling it out. Now we can also remove the pedestal and core cap.

- **Removing the core center:** We then place the mat in a container filled with water and let it **dissolve** the core center.

- **Finalizing the mat:** After the core center is dissolved we can place the coil with its heatsink inside the trap and screw the cover on.

Different prototypes required some different **additional clean-up** steps to remove some silicone excess.
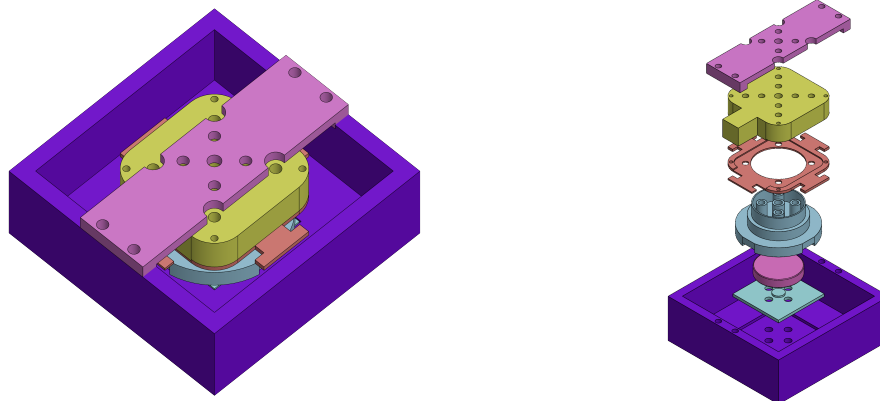
(A) View of the complete mold.

(B) Exploded view of the complete mold.

FIGURE 5.25: Complete mold for the mat.

5.3.3 Design faults and problems

Membrane fragility

As we previously touched on in paragraph 5.3.1, the membrane arms tend to **break** at the connection with the **cylindrical chamber**. This is due to the abrupt change of profile that causes a stress concentration at that point. This problem was especially noticeable during testing, as we had to **remove the magnet** from the chamber **multiple times** damaging the structure of the membrane. Adding some fillets to the connection between the arms and the chamber helped to solve this problem, but it didn't eliminate it. The good thing is that the membrane is **easily fixable** by adding very **small amounts of silicone** to the broken parts **as glue** and letting it cure.

Overall system flexibility

In the case of the small magnet, this design resulted in a **pretty flexible device** that could be bent a fair amount in all directions.
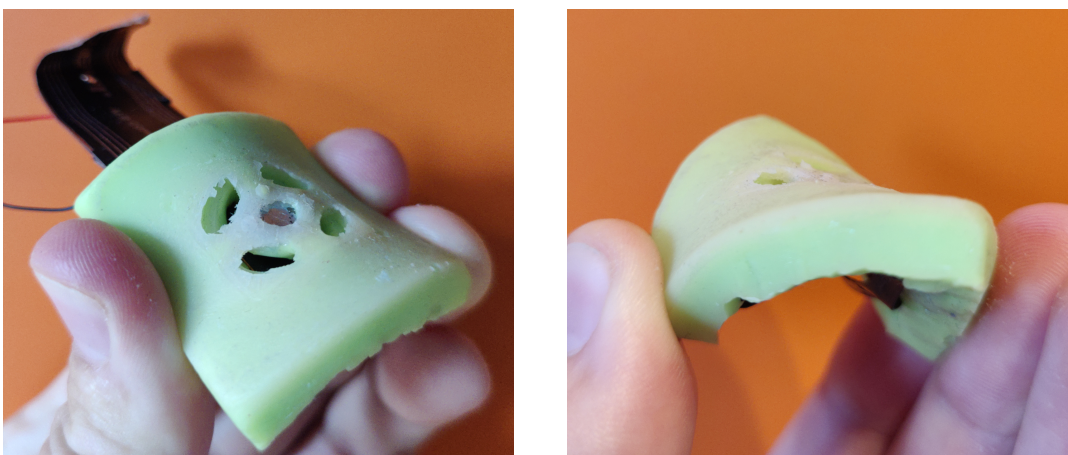
FIGURE 5.26: Flexible mat prototype bending.

Meanwhile, in the case of the big magnet, the mat was also pretty flexible but the magnet with its size **impeded the structure from bending as much as the small magnet version**.

Coil trap design faults

The main problem with the coil trap design was that **screwing** the two parts together is not **reliable**. As the two parts are connected by screws in only four points they tend to **separate when the mat is bent**. This is because the lower part follows the bending of the mat through its fins, these fins are not directly connected to the upper part.
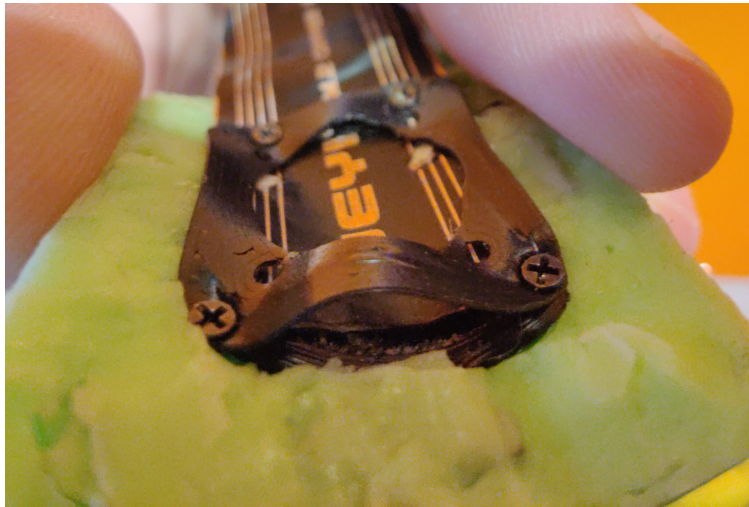
FIGURE 5.27: Coil trap separating when the mat is bent.

5.4 Experimentation and Evaluation

In this section, we will present the results of the **experiments** we conducted on the coil itself and the flexible mat prototypes. We will start by presenting the results of the **heating tests** we conducted on the coil. Then we will move on to the results of the **force response tests** we conducted on the flexible mat prototypes.

5.4.1 Heating testing

As we discussed in previous sections coils have a **critical issue with heating**. This is because the coil is a resistive element that generates heat when current flows through it. This is the main reason why the coil cannot produce very high magnetic fields and in turn high magnetic repulsion forces. With these tests, we wanted to understand the **limits** of **Flexar coils**, in this way, we wanted to reach an **optimal working point** and configuration for our prototypes. The configurations we tested were two, one considering only **one coil** and the other considering **two coils** connected in **parallel**. Both were then tested in **DC** and **AC** conditions.

For the **DC test**, the coils were connected to an **RND 320-KA300SP** bench power supply with which we did a voltage sweep from **0.5V** to **4V**, with **0.5V steps**.

Meanwhile, for the **AC test**, we used an **Agilent 33220A** function generator and a **Kepco BOP 20-10M** bipolar power amplifier. The power amplifier was set to amplify

the input signal with a **voltage gain of 10**. Two types of AC tests were conducted, both were done with sine waves at **20Hz**. In the first type, the function generator was set to output a bipolar sine wave from **-V_{max} to V_{max}**, with V_{max} being the voltage we wanted to test. In the second type, the function generator was set to output a **unipolar sine wave** from **0 to** V_{max}. Then we devised a voltage sweep **[0.5, 6]V** ([0.05, 0.6] on the signal generator) with **0.5V steps** for the V_{max}.

The voltage limits we chose were based on the **maximum voltage** the coil could withstand before reaching its **thermal runaway point**.

To measure the temperature of the coil we used a multimeter connected to a **thermocouple**. The coil/s were placed on a piece of wood to **avoid heat dissipation** through the table, and the thermocouple was placed on top of the coil/s. To keep both in place they were **taped to the wood** with electrical tape.
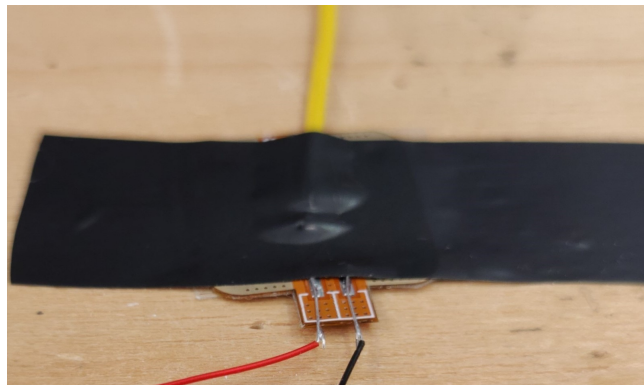
FIGURE 5.28: Heating test setup.

Single coil tests' results

The results of the **single coil** tests are shown in figure 5.29.
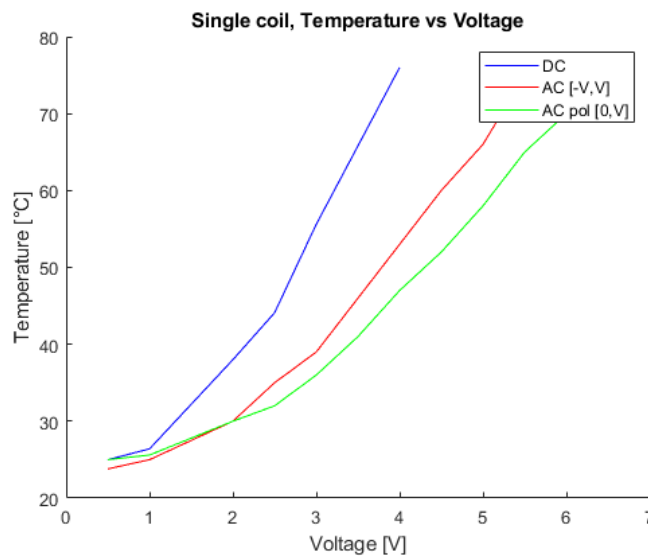
FIGURE 5.29: Temperature vs Voltage for one coil.

As we can observe the coil tends to heat up **way less** in **AC** conditions, especially in the **unipolar case**. This is due to the **lower RMS value** of the current that flows through the coil in AC conditions.

Two coils in parallel tests' results

The results of the **two coils in parallel** tests are shown in figure 5.30.
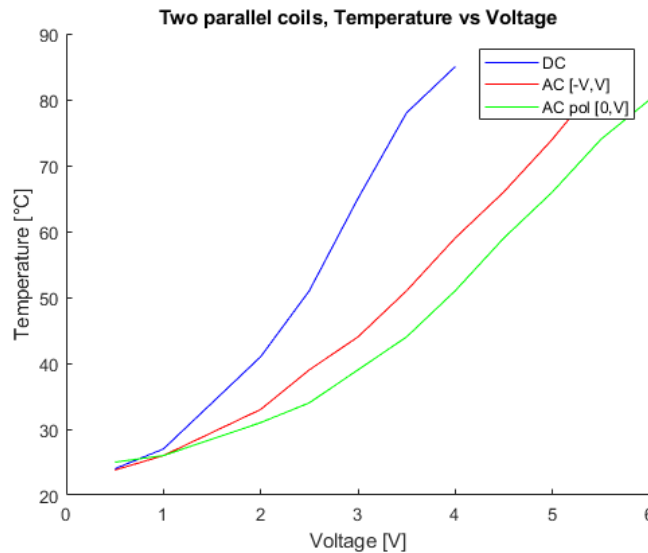
FIGURE 5.30: Temperature vs Voltage for two coils in parallel.

This case is comparable to the previous one, but here the two coils in parallel tend to **heat up more** than the single coil even if the current is divided between the two coils. This is because the two coils are **glued together** and the heat generated by one coil is **transferred** to the other one.

5.4.2 Force testing

The force testing was conducted on the **flexible mat prototypes**. The goal of these tests was to understand the relationship between the **force** generated by the coil and the **voltage** applied to it. To measure the force generated by the coil we used an **ATI TW-Nano17** force sensor. As we needed to measure the force in the z direction we had to create a way to **suspend the sensor** above the mat membrane. This mount should also allow the sensor's **position to be adjusted on the z-axis** to be able to position the sensor at the right height **to not press the membrane too much**. We modeled the structure based on the 3D model of the ATI sensor and then 3D printed its various components.
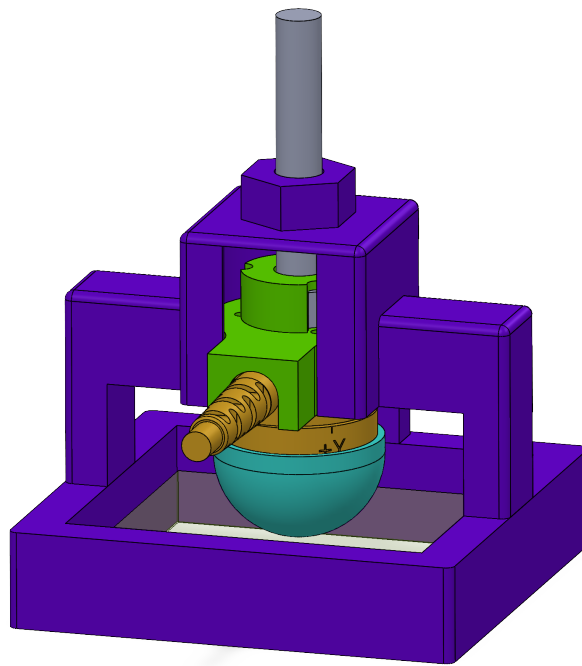
FIGURE 5.31: Sensor mount complete structure.

The structure is composed of 3 3D printed PLA components, one nut and a bolt. The components are the following:

- **Sensor mount:** this component holds the sensor and houses the bolt head on its top. It was designed to trap the head of the bolt but to leave it able to rotate, this was done by temporarily **pausing the printing process** and inserting the bolt. Then the printing process was resumed to create the blocking layers on the bottom of the bolt's head. (Green component in figure 5.31)
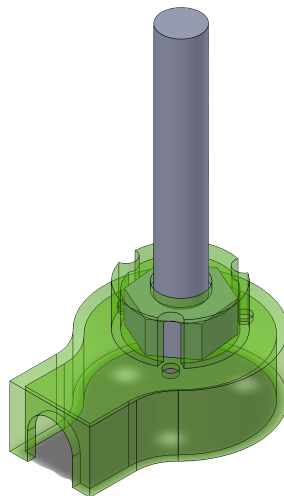
FIGURE 5.32: Sensor mount see-through view.

- **Sensor mount base:** this component is the base of the structure, on the bottom has a squared hole where the **flexible mat** can be inserted and on the top houses a nut **trapped in the print** to allow the bolt to be screwed up and down. (Purple component in figure 5.31)
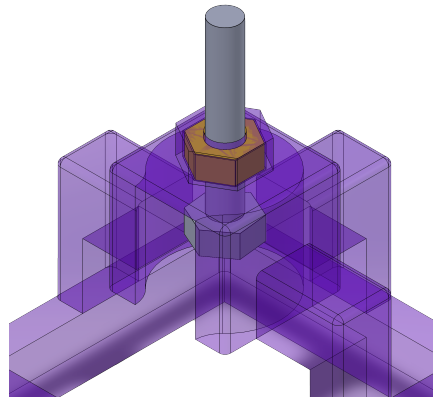
FIGURE 5.33: Sensor mount base see-through view of the nut and bolt mechanism.

- **Sensor's pulp:** this component is mounted below the sensor and is used to press the membrane of the mat on a **small area**, to **simulate a finger** pressing on the mat. (Teal component in figure 5.31)

The complete test setup is shown in figure 5.34.
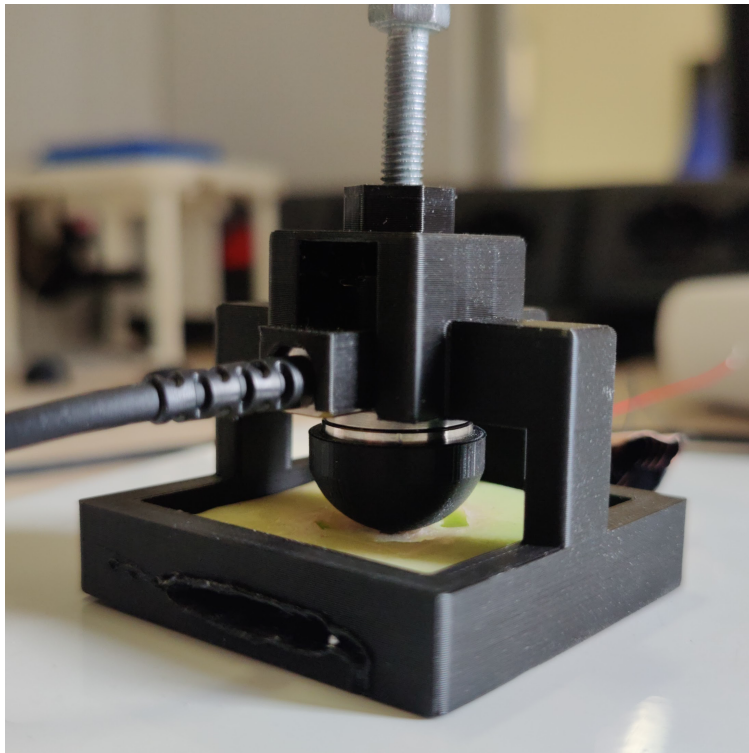
FIGURE 5.34: Complete force testing setup.

ATI data acquisition was done with a **MATLAB script** based on the work of [25].

ATI sensor low sensitivity

After some tests, we quickly realized that the ATI sensor was **not sensitive enough** to measure the forces generated by the mat prototype when driven with **sinusoidal signals**. This is because, even at the max rated voltage we can drive the coil with (6V), the magnetic field generated by the coil is **not strong enough** to generate a magnetic repulsion force with the magnet that can be measured by the sensor. The only way to measure the force generated by the coil is to make it produce a way **higher magnetic field**, the solution we found was to use a **signal with very high peaks but low RMS voltage**. In this way, the coil can generate high peaks of magnetic field for a **short time**, enough to generate a force that can be measured by the sensor without producing too much heat. A good candidate for testing with this type of signals is the **heartbeat pulse**, it presents a very **high peak** at the ventricles contraction and then a **low value** during the rest of the heartbeat cycle.
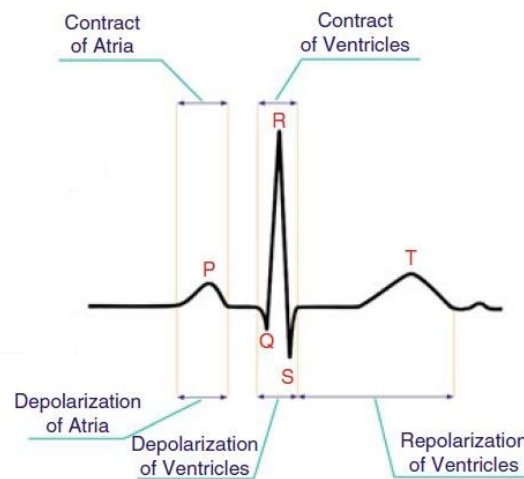
FIGURE 5.35: Heartbeat pulse.

We chose the heartbeat because it's a good example for our case study as it is a **low-frequency signal** and because we managed to run the coil with it even at up to **30V peak** value without reaching its thermal runaway point. Also, the simulated heartbeat was **easily recognizable** by the subjects who tested the flexible mat prototype.

Testing procedure

To measure the force generated by the mat prototypes we used an **automatic testing** procedure controlled by a **MATLAB script**. The computer running the script was connected to the **function generator** and the **ATI sensor**. The script was designed to:

- **Set** the function generator to output the desired **signal**, **voltage** and **frequency**.

- **Measure** the force offset on the sensor when the coil was off.

- **Turn on** the signal on the function generator.

- **Read the sensor data** for a given amount of seconds, with a given number of samples.

- **Turn off** the signal.

Then the script would **plot the force data** and **save it** to a file.

Magnet size vs Force

The main reason we decided to carry out this test was to **compare** the force generated by the two mat prototypes we developed, the one with the **small magnet** and the one with the **big magnet**. We tested them both using two coils in parallel and the **heartbeat pulse signal** at **30V peak** value.

The results of the tests are shown in figure 5.36.
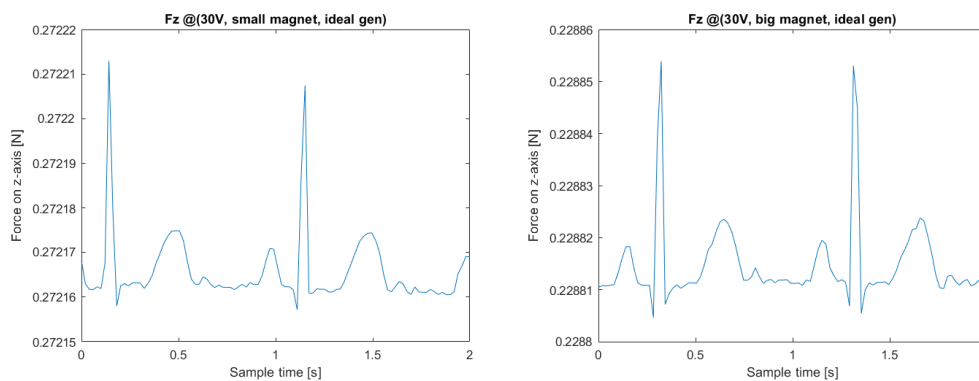
(A) Force profile of the small magnet prototype.   (B) Force profile of the big magnet prototype.

FIGURE 5.36: Force profile of the two mat prototypes run with the heartbeat pulse signal.

As we can see the force generated by the two prototypes is **comparable**, but sadly the **force generated by the big magnet prototype is lower** than the one generated by the small magnet prototype.

In both cases we can observe that the force never reaches $0N$, this is because we always have the **membrane pressing on the sensor**, resulting in a **constant offset** of about **0.2N**. Removing the offset we can obtain that the **net force** generated by the prototypes is in the order of $5 \cdot 10^{-5} N$.

Chapter 6

Conclusions and Future Work

6.1 Conclusions

6.1.1 Low force output

In the previous chapter, we measured the **maximum force** our system could generate in the **best conditions**. Even **overloading** the coil for short bursts of **30V** we achieved a measle $5 \cdot 10^{-5}$**N** of force 5.4.2. Considering the **small magnet prototype** (**1.03g** mass), this means we have generated an **acceleration** of about **0.05m/s²**. The **application area** is about **78.54mm²**, so considering what we discussed in paragraph 3.1.2, the prototype couldn't even reach the haptic sensitivity of human fingers (**[0.1778-0.5623]m/s²**).

Test subjects were **anyway able to feel some vibrations**, we can theorize that the sensitivity threshold was **lowered** by the **constant pressure force** applied on the skin by the **membrane (0.2N)**, this is also supported by the study in paragraph 3.1.2. Even still the vibrations were **very weak** and **barely perceptible**.

6.1.2 Alternative signals

We also tested other **low RMS signals** with **high peaks** to see if we could simulate **other sensations** besides the heartbeat. We tested the sound of **gunshots**, the sound of a **bell ringing** and the sound of a **thunder strike**. The best result was achieved with the thunder strike, the **big peak** created a **satisfying vibration** and we could even tell somewhat the consequent **rumbles**. The only problem was that subjects **weren't able to recognize what the vibration was supposed to represent** without being told beforehand, that wasn't the case with the heartbeat.

6.1.3 A technology not suitable for haptic feedback devices

As we discussed multiple times in this thesis, driving these low-resistance flexible coils with **AC signals** is very **difficult** and **inefficient**. The complex circuitry required to drive these coils is not only **expensive** but also **difficult to design and tune**. The high power consumption is also a major drawback. Combining all these factors with the low magnetic field output, we can conclude that this technology is **not ready for mainstream application in haptic feedback devices**.

6.2 Alternative applications

The most promising application for flexible PCB coils is using them as very **thin electromagnets**. By combining them with **high magnetic permeability materials**, we could increase substantially their **magnetic field output** 2.1.3. Usually, high-permeability materials are metals so we could also exploit their **high thermal conductivity** to **dissipate the heat** generated by the coils, allowing us to increase the coil power input and in turn their magnetic field output. Some tests in this direction have already been done in the past [26].

Meanwhile, a very interesting application for standard PCB coils is PCB stator axial electric motors. This type of motor has multiple advantages over traditional electric ones:

- **Very thin** and **lightweight** stators.

- **Very low inertia**, allowing for very **fast response times**.

- **High efficiency**.

- **Lower cost** and **material waste** as we have no need for copper windings.

- **High reliability** as windings are usually prone to **mechanical failure**.

- **Ease of repair** as we can easily replace the PCB.

- **Easy customization** as by changing the stator PCB design, one can modify the **torque-speed curve** of the motor and **size** of the motor. Also by increasing the **number of layers of the PCB**, we can increase the stator **magnetic field output**.
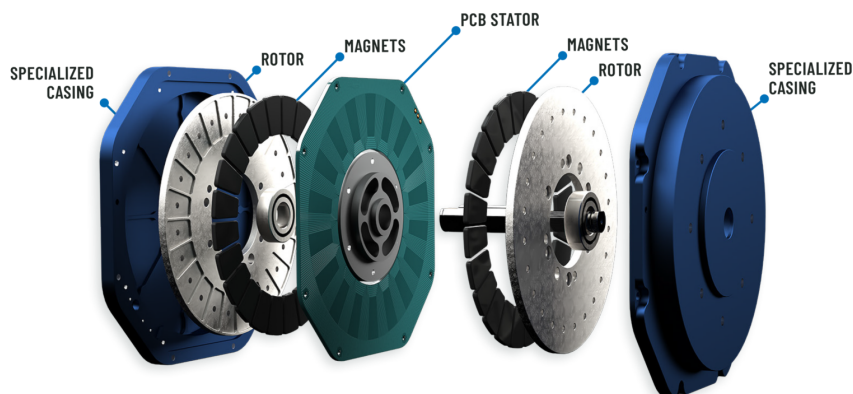
FIGURE 6.1: Explosion view of a PCB stator axial motor from PCB Stator [27].

6.3   Future work

Some effort could be put into **optimizing the coil design** for haptic feedback applications. We could especially focus on **increasing the magnetic field output** of the coils and optimizing the **magnetic field coupling** with the magnet.

6.3.1   Custom coil design

As we previously briefly touched on, PBC coils can be designed with **very different traces design** in mind 2.2.1. One way to exploit this could be to **increase the number of spires in the same area**, increasing the magnetic field output. For example, considering Flexar coils, we could use a **square pattern** for the traces to increase the number of spires in the same area. Then we could substitute the cylindrical magnet with a **parallelepiped one**, to increase the m**agnetic field coupling with the coil**.

This is all speculation in fact, it could be wise to first due some **FEM simulations** to test the feasibility of this idea.

Bibliography

[1] K. Kawabe, H. Koyama, and K. Shirae. "Planar inductor". In: *IEEE Transactions on Magnetics* 20.5 (1984), pp. 1804–1806. DOI: 10.1109/TMAG.1984.1063271.

[2] Jonsenser Zhao. "A new calculation for designing multilayer planar spiral inductors". In: *Edn -Boston then Denver then Highlands Ranch Co-* 55 (July 2010), pp. 37–40.

[3] The Engineering ToolBox. *Length of a Spiral*. https://www.engineeringtoolbox.com/spiral-length-d_2191.html [Accessed: 22/04/2024]. 2021.

[4] Minh Nguyen and Handy Blanchette. "Optimizing AC Resistance of Solid PCB Winding". In: *Electronics* 9 (May 2020), p. 875. DOI: 10.3390/electronics9050875.

[5] Christian Østergaard et al. "Simulation and measurement of AC resistance for a high power planar inductor design". In: *2019 IEEE 13th International Conference on Compatibility, Power Electronics and Power Engineering (CPE-POWERENG)*. 2019, pp. 1–5. DOI: 10.1109/CPE.2019.8862361.

[6] Minh Nguyen and Handy Blanchette. "Optimizing AC Resistance of Solid PCB Winding". In: *Electronics* 9 (May 2020), p. 875. DOI: 10.3390/electronics9050875.

[7] supermagnete.de. *Magnetic field of various permanent magnets*. https://www.supermagnete.de/eng/faq/How-do-you-calculate-the-magnetic-flux-density.

[8] Wikipedia. *Magnetic levitation between magnet and serpentines*. Accessed: 09/07/2024. URL: https://en.wikipedia.org/wiki/Magnetic_levitation#2D_Movement.

[9] Dr. Minas E. Lemonis. *Statics of fixed beams*. https://calcresource.com/statics-fixed-beam.html.

[10] A. Khurshid, Abdul Ghafoor, and Afzaal Malik. "Robotic Grasping and Fine Manipulation Using Soft Fingertip". In: Aug. 2011. ISBN: 978-953-307-373-6. DOI: 10.5772/23697.

[11] Gaetan Boyer et al. "In vivo characterization of viscoelastic properties of human skin using dynamic micro-indentation". In: *Conference proceedings : ... Annual International Conference of the IEEE Engineering in Medicine and Biology Society. IEEE Engineering in Medicine and Biology Society. Conference* 2007 (Feb. 2007), pp. 4584–7. DOI: 10.1109/IEMBS.2007.4353360.

[12] Nicole D'Aurizio. "Algorithms and Wearable Technologies Enabling Haptic Communication". Available at https://hdl.handle.net/11365/1225277. PhD thesis. University of Siena, Jan. 2023.

[13] Stefano Papetti et al. "Vibrotactile Sensitivity in Active Touch: Effect of Pressing Force". In: *EEE Trans. Haptics* 10.1 (Jan. 2017), pp. 113–122. ISSN: 1939-1412. DOI: 10.1109/TOH.2016.2582485. URL: https://doi.org/10.1109/TOH.2016.2582485.

[14] John Wu et al. "Finite element analysis of the penetrations of shear and normal vibrations into the soft tissues in a fingertip". In: *Medical engineering & physics* 29 (July 2007), pp. 718–27. DOI: 10.1016/j.medengphy.2006.07.005.

[15] *Piezo Haptic Actuator - PowerHap*. PowerHap 15G. TDK. 2017. URL: https://www.mouser.com/datasheet/2/400/PowerHap_15G-1144538.pdf.

[16] piezodrive.com. *Piezo Actuator Power Calculator*. `https://www.piezodrive.com/piezo-actuator-power-calculator/`.

[17] corz.org. *ESP32 Signal Generator*. `https://corz.org/ESP32/square-sine-triangle-wave-signal-generator`.

[18] *L272: Dual Power Operational Amplifier*. L272. STMicroelectronics. 2003. URL: `https://www.st.com/resource/en/datasheet/l272.pdf`.

[19] HZDR. *HZDR - Helmholtz-Zentrum Dresden-Rossendorf*. `https://www.hzdr.de`.

[20] microbots. *microbots Company*. `https://www.microbots.io`.

[21] Carl Bugeja. *LinkedIn Profile*. `https://www.linkedin.com/in/carl-bugeja-0b922a135/`. Accessed: 2024-05-27. 2024.

[22] Peter Johnson and Janet Blackstone. "Children and gender - Differences in exposure and how anthropometric differences can be incorporated into the design of computer input devices". In: *SJWEH Supplements* 33 (Jan. 2007).

[23] ResChimica. *R Pro 10 Silicon*. `https://www.reschimica.com/it/gomme-siliconiche/121-227-r-pro-10-gomma-siliconica-liquida-per-stampi-morbidi.html`.

[24] ResChimica. *R Pro Fast Silicon*. `https://www.reschimica.com/it/gomme-siliconiche/119-222-r-pro-fast-gomma-siliconica-per-prototipazione-rapida.html`.

[25] LuSeKa. *ATI NetFT Matlab Interface*. `https://github.com/LuSeKa/ATI_NetFT_MatlabInterface`. Accessed: 26/06/2024. 2018.

[26] Carl Bugeja. *Flexar as Electromagnets*. `https://www.youtube.com/watch?v=XfVz9Otxzyo`. 2021.

[27] PCB Stator. *PCB Stator company*. `https://pcbstator.com/`. Accessed: 26/06/2024.

Acknowledgements

the fog is coming